Chapter 6
Special Problems

Francesca Ceroni, Marisa Pecce, Christian Carloni, Thorsten Leusmann, Harald Budelmann, Emidio Nigro, Antonio Bilotta, Joaquim Barros, Inês Costa, Gian Piero Lignola, Annalisa Napoli and Roberto Realfonzo

Abstract This chapter gives an overview on the state-of-the-art about verifications of reinforced concrete structures using Externally Bonded (EB) Fibre Reinforced Polymers (FRP) under particular loading condition. Focus is mainly put on flexural strengthening, nowadays the most common application field for composite materials in structural engineering. The items discussed in this chapter are:

- Serviceability limit states;
- Fatigue behaviour;
- Effects of fire and high temperature;
- Long term behaviour;
- Anchoring systems;
- Mechanically Fastened Systems.

F. Ceroni (✉) · M. Pecce (✉)
University of Sannio, Benevento, Italy
e-mail: ceroni@unisannio.it

M. Pecce
e-mail: pecce@unisannio.it

C. Carloni
Department of Architecture, University of Hartford, Hartford, USA

T. Leusmann · H. Budelmann
Institute for Building Materials, Concrete Structures and Fire Protection, TU Braunschweíg, Germany

E. Nigro · A. Bilotta
University Federico II, Naples, Italy

J. Barros · I. Costa
University of Minho, Mino, Portugal

G.P. Lignola
University of Napoli Federico II, Naples, Italy

A. Napoli · R. Realfonzo
University of Salerno, Salerno, Italy

C. Pellegrino and J. Sena-Cruz (eds.), *Design Procedures for the Use of Composites in Strengthening of Reinforced Concrete Structures*, RILEM State-of-the-Art Reports 19, DOI 10.1007/978-94-017-7336-2_6

Keywords FRP · Serviceability · Fatigue · Anchoring systems · Durability

Serviceability Limit States

Introduction

Both excessive cracking and excessive deformations in reinforced concrete elements may lead to drawbacks in service. *Appearance, tightness and durability* are normally considered as reasons for crack control. For durability considerations, the crack width in the vicinity of reinforcement is more influential than the crack width on the surface of the element. Cracking analysis of reinforced concrete elements externally bonded with FRP can be carried out considering the same principles of reinforced concrete sections.

In particular the cracks may decrease the durability performances, functionality and appearance of the structure or may endanger the integrity of the bond interface between FRP EBR and concrete.

The limitation of tensile stresses in concrete is an adequate measure to reduce the probability of cracking in tension. The limitation of compressive stresses in concrete aims to avoid or limit excessive compression, producing irreversible strains, longitudinal cracks (parallel to the compressive strains) and nonlinear creep phenomena.

In calculating the stress conditions, account shall be taken of whether the section is expected to crack under service loads. Moreover the effects of creep, shrinkage, relaxation of pre-stressing steel and differential temperatures should be taken into account.

The limitation of tensile stresses in the steel is an indirect method to control the cracks conditions in RC elements, since it is aimed to warrant an appropriate safety margin below the yield strength and, thus, prevent uncontrolled, large, permanently open cracks due to inelastic deformations of steel bars.

Finally, the deformability limit state has to be considered, because the limitation of deflections in RC elements is generally applied since excessive deflections may restrict the normal use of the structure, induce damage to not load-bearing members or negatively influence the appearance.

For RC elements, stresses are calculated using section properties corresponding to either the un-cracked or the fully cracked condition depending on the loading conditions. Both concrete and steel are assumed to be elastic, both in tension and in compression. When an external FRP reinforcement is present, it has to be considered as linear elastic. Thus, the calculation of stresses in concrete and steel follow the same rules used for RC elements under serviceability loading conditions, with the only difference of taking into account the external reinforcement in the analysis of the un-cracked and/or the fully cracked section.

Few test results are available for verification of serviceability limit states of RC elements strengthened with FRP EBR; most of tests available in literature have been carried out with reference to ties elements (Matthys 2000; Sato et al. 2002; Ueda et al. 2002; Zhang et al. 2003; Ceroni et al. 2004) and the codes do not always include design formulas.

Moreover, an increase in the load-carrying capacity by applying FRP laminates is not accompanied by a proportional increase in system rigidity, either in global terms (with reference to the values of deflections), or in local terms (with reference to the transfer of stresses at the FRP-concrete interface). Furthermore an increase of the ultimate capacity of an RC member due to the FRP strengthening does not correspond necessarily to a proportional increase of the service load; hence verification of serviceability could be significant in element design.

Since FRP materials have high tensile strength and Young's moduli, but small cross-sectional areas, in general their effect on the limitation of deflections can be negligible, unless considering very low reinforced section.

A more significant influence on the cracking pattern due to the local bond transfer produced by the external reinforcement can be observed (Ceroni and Pecce 2004).

Clearly, the use of pre-stressed FRP systems can be more and more useful to reduce the width of existing cracks, limit the deflections and control the stresses in critical sections of structural RC members (Kim et al. 2008).

Stress Limitation

Load combinations for verifications at SLS as specified in Eurocode 2 (EN 1992-1-2 2004) should be applied. Partial safety factors for the materials, γ_M, are taken equal to 1.0, except if specified otherwise.

Under the hypothesis that the section remains plane, the strains in the steel and in the FRP reinforcement are related to the concrete strains thanks to a linear relation. Due to the assumption of linear elastic behaviour for all materials, the stresses are obtained multiplying the strains by the elastic modulus. In particular, the stress in the FRP is obtained from the following relationship:

$$\sigma_f = E_f \cdot \varepsilon_f \tag{6.1}$$

where E_f is the mean value of the modulus of elasticity of the FRP reinforcement.

Moreover, existing strain at the time of FRP installation shall be accounted for and the principle of superposition can be used.

If the maximum tensile stress in the concrete is lower than its tensile strength, the section is un-cracked and fully active; on the contrary the section should be treated as cracked.

The modular ratios $\alpha_s = \frac{E_s}{E_c}$ and $\alpha_f = \frac{E_f}{E_c}$ have to be defined to transform the actual section into a homogenized all-concrete section. These values shall be set to account for creep as well as short and long-term conditions. In particular, under permanent loading conditions, a reduced value of the elastic modulus of concrete can be used to take into account the creep effect, while under not-permanent loading conditions the ratio of the effective moduli can be used.

For calculating the strain and stress distribution along the section a linear elastic analysis both of the un-cracked (state 1) and cracked section (state 2) should be carried out.

To this aim the cracking moment, M_{cr}, for a rectangular section with base b and height h, can be evaluated as:

$$M_{cr} \approx f_{ctm} \cdot \frac{b \cdot h^2}{6} \tag{6.2}$$

where f_{ctm} is the mean tensile strength of concrete [MPa]. If M is the rate of maximum moment in the element under the service loading conditions applied after the strengthening and M_0 is the moment applied before the strengthening, the stresses induced in the materials by the overall moment $M_k = M_0 + M$ can be evaluated adding the contributes of both moments.

If M_o is higher than M_{cr}, the analysis can be developed referring to the cracked inertia (state 2) of the section for calculating both the stresses in concrete and steel reinforcement under M_o and the stresses in concrete, steel and FRP reinforcement under M; the total stress in concrete and steel is the sum of the two contributions.

On the contrary, if M_0 is lower than the cracking moment M_{cr} and the total moment M_k is greater than M_{cr}, the inertia of the un-cracked section has to be used for calculating the stresses in concrete and steel reinforcement under M_0, while the cracked inertia has to be used for calculating the stresses in concrete, steel and FRP reinforcement under M.

The case of both values M_0 and M_k lower than M_{cr} can be considered not significant for the usual applications.

When cracking has to be avoided, a limit state of decompression can be assumed for verifications and corresponds to have a zero stress at the extreme fibre of the concrete section.

The compressive stresses in the concrete should be limited to $0.6 \cdot f_{ck}$ under the characteristic combination of loading and $0.45 \cdot f_{ck}$ under the most unfavourable quasi-permanent load combination.

About the limitations of the tensile stress in the steel reinforcement, under the characteristic combination of actions the limit $0.8 \cdot f_{yk}$ should not be exceeded.

The stress limit above introduce are in agreement with the indications of Eurocode 2.

The FRP stress under service load should be limited in order to avoid excessive creep or creep rupture of the FRP:

$$\sigma_f \leq \eta \cdot f_{fk} \tag{6.3}$$

for the most unfavourable quasi-permanent load combination.

The FRP stress limitation coefficient, $\eta < 1$, depends on the type of FRP and should be obtained through experiments. The Italian Guidelines (CNR DT 200/R1 2012) suggest the following ranges depending on the type of fibres: 0.75–0.95 for internal environment, 0.65–0.85 for external environment, and 0.50–0.85 for aggressive environment. The lower values are for glass fibres and the upper for carbon fibres. The same values are furnished also in ACI 440.2R-08.

Control of Cracking Phenomena

Limitation of Longitudinal Cracks

Application of the FRP reinforcement substantially changes the cracking scenario of the element, since tension stiffening phenomena develop not only at the steel-concrete interface, but also at the FRP-concrete interface. In RC elements strengthened with FRP, the crack width is thus generally smaller than for unstrengthened elements either considering the same service load or considering the same tension level in the steel, due, in both cases, to the additional tension stiffening of the external reinforcement that reduces the crack spacing. Since new cracks will appear in between existing cracks, in general, a more diffuse crack patterns, with smaller crack widths, are observed.

A real crack bridging effect due to the external FRP reinforcement has been observed in experimental tests with a further tension stiffening effect in addition to the one produced by the internal steel reinforcement (Yoshizawa and Wu 1999; Tripi et al. 2000; Matthys 2000; Ueda et al. 2002; Ceroni et al. 2004; Ceroni and Pecce 2007; Ferrier et al. 2003). Moreover as the stiffness of the FRP strengthening grows the global tension stiffening results considerably increased. In Ceroni and Pecce (2007), bending tests on beams externally bonded both with carbon and steel cords sheets were carried out and evidenced that: (1) the steel cords and carbon fibres, both impregnated with epoxy, gave very similar results when the equivalent reinforcement percentage was the same, (2) when the steel cords were bonded with cementitious grout, the tension stiffening effect was lower compared with the epoxy.

Modelling of tension stiffening in RC elements is based on many experimental tests and on a consolidated knowledge of the steel–concrete bond. On the contrary the tension stiffening effect and the cracking behaviour has not been well investigated yet for RC elements externally bonded with FRP, due also to the lack of experimental results concerning this aspect. Numerical models taking into account the tension stiffening effects of the external FRP reinforcement can be used to

predict the crack width (Ceroni and Pecce 2004; Aiello and Ombres 2004; Ferretti and Savoia 2003). However for design purposes, empirical equations based on regression analysis of experimental data can be obtained to calculate directly the crack width (Tan and Saha 2008) or the crack spacing (Ceroni and Pecce 2009).

Applying the technical report (fib bulletin 14 2001) the crack width can be estimated by using the Model Code approach (Model code 90) and a specific formula is furnished for the crack spacing for taking account the external FRP reinforcement.

$$\begin{aligned} s_{rm} &= \frac{2 \cdot f_{ctm} \cdot A_{c,eff}}{\tau_{fm} \cdot u_f + \tau_{sm} \cdot u_s} \\ \tau_{s,m} &= 1.8 \cdot f_{ctm} \quad \tau_{f,m} = 1.25 \cdot f_{ctm} \end{aligned} \tag{6.4}$$

where f_{ctm} is the mean tensile strength of concrete [MPa], u_s and u_f are the perimeter of the steel bar and FRP laminates [mm] bonded to concrete, t_f the thickness of FRP [mm], $\tau_{s,m}$ and $\tau_{f,m}$ the bond stresses [MPa] along the steel-concrete and the FRP-concrete interfaces, assumed constant in s_{rm}.

According to American guidance ACI 440.2R-08, verification of cracking under service loads can be done by applying the provisions of ACI 318-11 (2013) for RC elements. The FRP external reinforcement has to be taken into account in the calculation of the inertia of the transformed section. In particular in (ACI 318-95) an empirical formula is proposed to evaluate directly the maximum crack width, w, without evaluating crack spacing:

$$w = 2 \cdot \frac{f_f}{E_f} \cdot \beta \cdot k_b \cdot \sqrt{d_c^2 + \left(\frac{s}{2}\right)^2} \tag{6.5}$$

where E_f and f_f are the modulus of Young and the tensile stress in the steel reinforcement, respectively, k_b is a bond parameter, experimentally calibrated at 1 for ribbed steel, β is the ratio of distance between neutral axis and tension face to distance between neutral axis and centroid of internal reinforcement, d_c is the concrete cover, s is the bar spacing. The presence of the external reinforcement is taken into account only in the calculation of the inertia.

Currently in the Italian Guidelines (CNR DT 200/R1 2012) no specific formulas are available for calculating crack width in RC elements externally bonded with FRP materials, but only general indications referring to well-known approach as the one proposed by Model Code or Eurocode 2.

Under a stabilized cracking condition, the indications given by Eurocode 2 (EN 1992-1-2 2004) and the new Model Code (MC 2010) for RC elements can be, indeed, extended to RC elements externally bonded with FRP materials. Verification of serviceability in the new Model Code for RC elements includes again a cover term in the crack spacing formula in order to emphasize possible deformations in the concrete cover. The cracking model kept the philosophy that the maximum crack width (called herein as design crack width) is the multiple of $2 \cdot l_{s,max}$ (slip lengths) and the average strain differences between two cracks.

According to the new Model Code, the design crack width, w_d may be calculated by:

$$w_d = 2 \cdot l_{s,\max} \cdot (\varepsilon_{sm} - \varepsilon_{cm} - \varepsilon_{cs}) \tag{6.6}$$

$$l_{s,\max} = k \cdot c + \frac{1}{4} \cdot \frac{f_{ctm}}{\tau_{bms}} \cdot \frac{\phi}{\rho_{s,ef}} \tag{6.7}$$

$$\varepsilon_{sm} - \varepsilon_{cm} = \frac{\sigma_s - \beta \cdot \sigma_{sr}}{E_s} = \frac{\sigma_s}{E_s} \cdot \left(1 - \beta \cdot \frac{\sigma_{sr}}{\sigma_s}\right) = \frac{\sigma_s}{E_s} \cdot \left(1 - \beta \cdot \frac{M_{cr}}{M_{\max}}\right) \tag{6.8}$$

where:

- σ_s is the steel stress in a crack,
- σ_{sr} is the maximum steel stress in a crack at the crack formation stage which for pure tension, defined as:

$$\sigma_{sr} = \frac{f_{ctm}}{\rho_{s,ef}}(1 + \alpha_e \rho_{s,ef}) \tag{6.9}$$

where:

$$\rho_{s,ef} = \frac{A_s}{A_{c,ef}} \quad \alpha_e = \frac{E_s}{E_c} \tag{6.10}$$

and $A_{c,ef}$ is the effective area of concrete in tension, defined as follows:

$$A_{c,ef} = b \cdot \min\left[2.5 \cdot c,\ \left(\frac{d-x}{3}\right),\ \frac{d}{2}\right] \tag{6.11}$$

b, d and c are the width, the depth and the inferior cover of the concrete element;

- β is an empirical coefficient to assess the mean strain over $l_{s,max}$ depending on the type of loading (0.6 for short term loads, 0.4 for long term loading);
- k is an empirical parameter to take the influence of the concrete cover into consideration; according to the present knowledge, k = 1.0 can be assumed;
- η_r is a coefficient for considering the shrinkage contribution;
- ε_{sh} is the free shrinkage strain.

Note that in Eurocode 2 (EN 1992-1-2 2004), the following provision for the maximum crack spacing is provided:

$$w_k = s_{r,\max} \cdot (\varepsilon_{sm} - \varepsilon_{cm}) \tag{6.12}$$

$$s_{r,\max} = 3.4 \cdot c + 0.425 \cdot k_1 \cdot k_2 \cdot \frac{\phi}{\mu_s} \tag{6.13}$$

$$\varepsilon_{sm} - \varepsilon_{cm} = \frac{\sigma_s}{E_s} \cdot -k_t \left[\frac{f_{ctm} \cdot A_{c,eff}}{E_s \cdot A_s} + \frac{f_{ctm}}{E_{cm}} \right] \tag{6.14}$$

- k_t a factor of load duration (0.6 for short and 0.4 for long term loading);
- k_1 is a bond coefficient: 0.8 for ribbed and 1.6 for smooth steel bars;
- k_2 takes into account type loading: 0.5 for flexural and 1.0 for tensile loading.

When FRP reinforcement is present, the percentage of reinforcement normalized to the effective area of concrete in tension can be modified as follows:

$$\rho_{eff,eq} = \rho_{p,eff} + \rho_{f,eff,eq} = \frac{A_s}{A_{c,eff}} + \frac{E_f}{E_s} \cdot \frac{A_f}{A_{c,eff}} \tag{6.15}$$

being A_s, E_s and A_f, E_f the area and the Young's modulus of the internal steel and the external FRP reinforcement, respectively.

Moreover, the expression of $2l_{s,max}$ can be calculated by means of specific formulae according to the type of FRP reinforcement. In particular, Ceroni and Pecce (2009) proposed a formulation for the average and the characteristic value of the crack spacing in RC elements externally bonded with FRP sheets. The formulation is empirically based on a best-fitting procedure considering experimental results about crack spacing according to a 'design by testing' procedure suggested in Eurocode 0 (EC0, Monti et al. 2009).

The database used for assessing the crack spacing is made by experimental results of RC beams and ties externally bonded with FRP sheets carried out by the authors in different experimental programs: beams (Ceroni and Pecce 2007; Ceroni 2010) and ties (Ceroni et al. 2004). The experimental results of these tests evidenced that at the same steel stress as more cracks form and the crack spacing is reduced, crack width decreases depending on the amount of external reinforcement that influences the total load applied. Considering the full load history, the tension stiffening effect due to the fibres grows for all the types of beams after the steel yielding due to the elastic behaviour of FRP. The external reinforcement produces the highest tension stiffening effect for beams with the lowest steel reinforcement. The greater the amount of FRP is used, the greater are the effects. In the tests on RC tie-specimens carried out according to the same dimensions and set-up used by Matthys (2000), a pre-load cycle established the crack spacing of the unstrengthened element and, after application of the external FRP reinforcement, new cracks formed about in the middle. Ceroni and Pecce (2009) made several comparisons in terms of crack spacing by defining a variable δ as the ratio of the code to the experimental value. For the provision given by EC2 (EN 1992-1-2 2004), where the FRP reinforcement is taken into account by the effective reinforcement percentage, the average value of δ is 0.48 meaning that the experimental values are overestimated; this can be justified by the assumption that

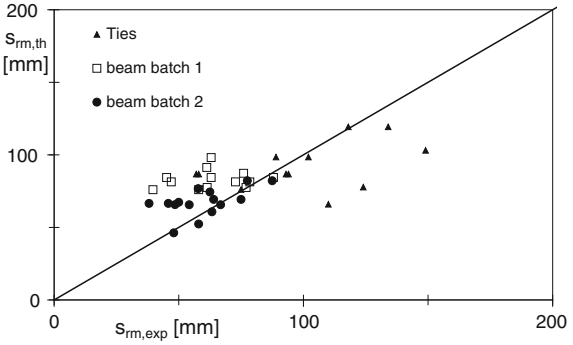

Fig. 6.1 Experimental versus theoretical average values of crack spacing given by Eq. (6.16)

such a formulation provided 'maximum' values of crack spacing. On the contrary, for the fib bulletin the mean value of variable δ is 2.14 which means a large underestimation of the experimental results.

The structure of the formulation proposed by Ceroni and Pecce (2009) for crack spacing is similar to Eq. (6.7) or (6.13) and the stiffening effect of the internal steel and the external FRP reinforcement is separately taken into account.

$$s_{rm} = s_0 + k \cdot \frac{A_{c,ef}^{\gamma} \cdot \phi^{\alpha}}{A_s^{\delta} + \left(\frac{A_f \cdot E_f}{E_s}\right)^{\beta}} \tag{6.16}$$

where s_0, k, α, β, γ and δ are parameters calibrated by the statistical procedure. In Fig. 6.1, the comparison between experimental and theoretical results given by Eq. (6.16) is reported assuming the following values of the parameters: $s_0 = 20$ mm, $k = 4$; $\alpha = 1$; $\beta = 0.75$; $\gamma = 0.5$; $\delta = 0.75$.

Equation (6.16) refers to the average value of the crack spacing, while for characteristic provision the following can be assumed:

$$s_{rm,th,k} = s_{rm,th,95\%} = 1.6 \cdot s_{rm} \tag{6.17}$$

In terms of crack width a more extended database was collected (107 data) by adding results of (Yoshizawa and Wu 1999; Matthys 2000). Equation (6.16) has been introduced in Eq. (6.12) for calculating the crack width: Fig. 6.2 shows the experimental-theoretical comparisons (mean values of δ = 0.777 and 0.715 for 64 and 107 data, respectively, CoV = 32 and 37 %).

On the contrary, the formulas of EC2 (EN 1992-1-2 2004) (Eqs. 6.12–6.14), adjusted to take into account the FRP external reinforcement, furnishes a mean value of δ = 0.67 (CoV = 50 %).

A model for considering the influence of NSM on the cracking is reported in (Zehetmaier and Zilch 2008) that based the formulation on experimental studies on NSM systems made of CFRP strips. The authors propose a modification both for

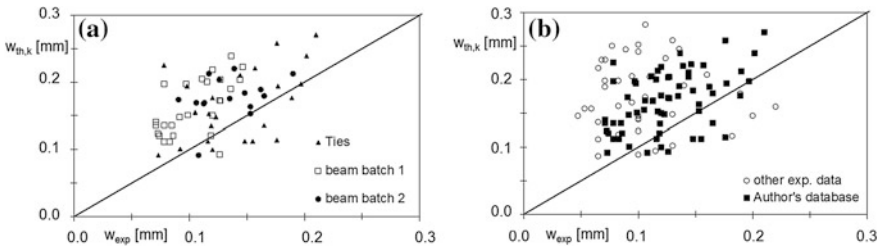

Fig. 6.2 Experimental versus characteristic theoretical values of crack width (Eqs. 6.12 and 6.16). **a** Authors' results, **b** extended database

the expression of the mean strain and the slip length in presence of NSM reinforcement.

In general, it is worth noticing that in reinforced concrete elements the spacing of internal stirrups can influence the crack spacing both with and without the FRP strengthening.

Verification of Bond Interface

Under service loading conditions, the initiation of bond interface cracks should be prevented as they may reduce the long-term integrity of the bond interface zone under e.g. cyclic loading and freeze/thaw actions. Concentrations of stresses develop especially at the end of the FRP reinforcement and the location of flexural or shear cracks.

At these locations, to avoid local debonding phenomena under the quasi-permanent load condition, the maximum principal stress, calculated based on the shear stress and the normal stress according to a linear elastic analysis (e.g. Taljsten 2004; Roberts 1989), should be smaller than the tensile strength of concrete.

According to the Italian guideline (CNR DT 200/R1 2012), the verification is developed checking that an equivalent tangential stress $\tau_{b,e}$ at the adhesive-concrete interface, under the rare or frequent load condition, is lower than the bond strength f_{bd} of the FRP strengthening–concrete interface. The equivalent tangential stress $\tau_{b,e}$ is defined through a mean tangential stress τ_m evaluated in the section at the FRP strengthening–concrete interface according to the Jourawski's formulation (Jourawski 1858) and a factor, k_{id}, that introduces by a simplified way the effect of the normal stresses.

The stresses have to be calculated under the only rate of loads applied after the adding of the FRP strengthening.

As in flexural strengthening, also in shear and torsion strengthening the externally bonded reinforcement shall not have debonding phenomena at the serviceability limit state.

Limitation of Deflections

The low axial stiffness $E_f A_f$ of FRP external reinforcement is often insufficient to reduce significantly curvatures and deflection in the strengthened beams under service load condition if the internal steel reinforcement is not yielded. On the contrary, a relevant stiffening effect is given by the external reinforcement, after the steel is yielded and is clearly proportional to the axial stiffness of the external FRP reinforcement (Ceroni et al. 2004). Also steel fabrics externally bonded to concrete beams (Balsamo et al. 2013a; Pecce et al. 2006) have evidenced an effectiveness into limiting the deflection after the yielding of internal steel reinforcement. Moreover, the bending tests reported by Balsamo et al. (2013b), evidenced that no significant difference was in using epoxy adhesive or cement-based mortar for impregnating the steel fabrics in term of deformability.

For the evaluation of deflections, the same method used for RC elements can be implemented to take into account the tension stiffening effect of both the internal and external reinforcement: (1) the most refined one is based on the double integration of the curvature, which can be determined by a cross-section analysis along the RC element; (2) a simplified calculation is based on the definition of an effective moment of inertia (Branson 1977; ACI 2005; El-Mihilmy and Tedesco 2000; Bischoff 2007) or on the calculation of a mean deflection according to the Eurocode (EN 1992-1-2 2004) and Model Code 2010 (fib bulletin 65 2012 and 66 2012) approaches.

The more refined procedure is able to take into account the tension stiffening effects in RC members due to both the internal and external strengthening based on the correspondent bond stress-slip laws (Ceroni and Pecce 2004; Aiello and Ombres 2000; Matthys 2000). Closed form equations have been also obtained assuming bi or tri-linear simplified moment–curvature responses (Razaqpur et al. 2000; Charkas et al. 2003; Rasheed et al. 2004).

The simplified formulation according to the Eurocode and Model Code approach is based on the calculation of the deflection in the FRP externally strengthened elements under the hypothesis of un-cracked and cracked section and on a 'tension stiffening coefficient' that synthesizes the tension stiffening phenomena along the element between two cracks due to both the internal and external reinforcement:

$$\alpha = \alpha_1 \cdot (1 - \zeta) + \alpha_2 \cdot \zeta \quad \zeta = 1 - \beta \cdot \left(\frac{\sigma_{sr}}{\sigma_s}\right)^2 \tag{6.18}$$

where:

- β is a coefficient taking into account the loading type (1.0 for single short-term loads and 0.5 for sustained loads or many cycles of repeated loading);
- σ_s is the tensile stress in the steel reinforcement under the service loading condition in the cracked section;

– σ_{sr} is the stress in the steel reinforcement calculated in the cracked section under the loading condition causing the first cracking (see Eq. 6.9).

The ratio σ_{sr}/σ_s may be replaced by M_{cr}/M for flexure and N_{cr}/N for pure tension, where M_{cr} is the cracking moment and N_{cr} is the cracking force and M and N are the maximum moment and normal force in the load combination considered.

The deflection at the un-cracked state, α_1, and the cracked state, α_2, can be calculated by an elastic analysis, referring to the flexural stiffness of the un-cracked section and the cracked state, respectively.

In the calculation of Eq. (6.18) the presence of the FRP external reinforcement has to be taken into account in the computation of the moment of inertia of the cracked section.

According to ACI 440.2R-08, the deflection under service loads can be calculated by applying the provisions of ACI 318-11 for RC elements. The FRP external reinforcement has to be taken into account in the calculation of the effective inertia, I_e, of the transformed section:

$$I_e = I_g \cdot \left(\frac{M_{cr}}{M_a}\right)^3 + I_{cr} \cdot \left[1 - \left(\frac{M_{cr}}{M_a}\right)^3\right] \tag{6.19}$$

where I_g and I_{cr} are the inertia of the un-cracked and cracked section, respectively, M_{cr} and M_a are the cracking and the maximum moment along the element.

In the case of NSM strengthening there are still few experimental results (Barros and Fortes 2005; Barros et al. 2007; Ceroni 2010; Balsamo et al. 2013b) to validate design formulations, but in general the same approach used for EBR systems can be assumed effective, introducing the specific modified moment of inertia. In particular, according to Ceroni (2010) and Balsamo et al. (2013b), the tension stiffening effect on the deflection provided by the NSM systems was founded to be less effective compared with the EBR technique. This was probably due to the application of the FRP reinforcement in the grooves that could lead to have higher slips along the FRP-concrete interface. In Fig. 6.3 the experimental load-deflection of the reference unstrengthened RC beams is compared with the curves of two equal beams strengthened with 2 and 3 CFRP strips, evidencing the low effect of the reinforcement on the beam stiffness.

Fatigue Behaviour

Introduction

Increasing traffic loads and aggressive environmental conditions are leading to an accelerated aging of reinforced concrete bridges and a loss in their load-carrying capacity. A well-established method to counteract effects of aging and increasing traffic loads is to strengthen bridges with fibre-reinforced polymers (FRP).

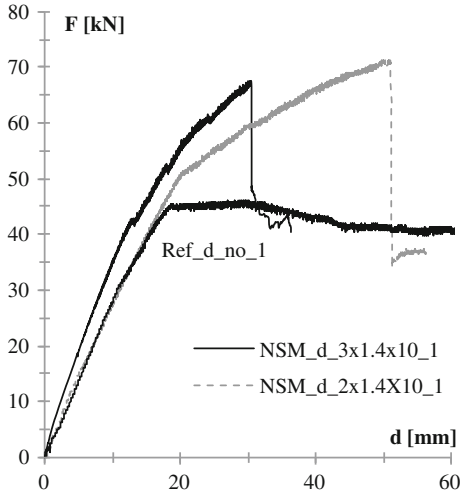

Fig. 6.3 Load-deflection curves of reference and NSM strengthened beams (Balsamo et al. 2013b)

With FRP strengthening, two objectives can be pursued: the increase of the load-carrying capacity and the extension of service life. The FRP material shows symptoms of fatigue when applied as an external reinforcement. The effect of cyclic loads on FRPs and hybrid FRPs is described in Wu (2010). Especially externally bonded FRPs (EBR) are affected by traffic induced vibrating and fluctuating loads, because cyclic loads also lead to a fatigue of concrete to FRP bond. The FRP debonding process under fatigue loading is the main objective in this chapter.

Experimental Tests

The debonding process of FRP under fatigue loading has been tested with different types of experimental tests. Commonly large scale bending tests at reinforced concrete beams strengthened with FRP under cyclic loading were carried out; see Heffernan (2004) and Kim (2008). In many cases fatigue loading leads to a failure of the interior reinforcing steel, in some cases FRP debonding could be observed followed by steel failure, see Kim (2008). If debonding is prevented, FRP strengthening leads to a higher load range or an increasing number of cycles at the strengthened RC beam, see Fig. 6.4.

According to Kim (2008), notable fatigue damage in FRP-strengthened beams is accumulated within the first cycles. The rate of damage accumulation then slows considerably until a linear damage rate is reached. Prior to fatigue failure of beams, rising damage propagation can be observed. The propagation of flexural cracks, maximum crack width, midspan deflection and steel strain show a similar trend.

These results are global measurements and do not attempt to directly evaluate the applied force in the external FRP reinforcement or the strain distribution along the

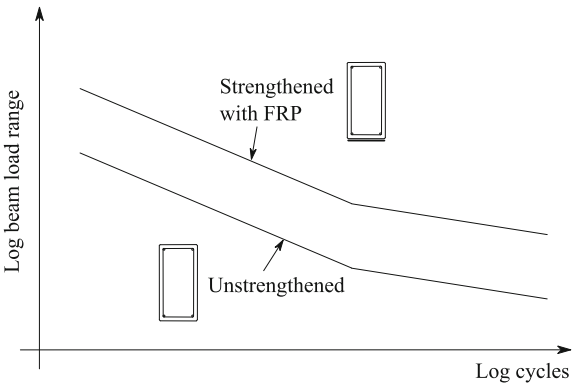

Fig. 6.4 Schematic of load range versus load cycle curves of RC beams according to Kim (2008)

fibres. Furthermore, the applied load range is not directly related to the load-carrying capacity of the interface, but rather to the load-carrying capacity of the beam. The published experimental work on the fatigue response of strengthened beams does not provide an insight into the fatigue response of the FRP-concrete interface.

A few studies, which directly investigate the fatigue response of the FRP-concrete interface using direct-shear tests of FRP-concrete joints, have been reported in Bizindavyi et al. (2003), Budelmann (2013), Carloni (2012, 2013), Dai (2005), Diab (2009), Ferrier (2005) and Ko (2007). The maximum, F_L^O, and minimum, F_L^U, load of the fatigue cycle are defined as a percentage of the load-carrying capacity of an equivalent specimen under monotonic quasi-static conditions. The available literature suggests that the fatigue response depends on the load range, mean value, and frequency.

The most common test set-ups for direct-shear tests are described in Yao (2005). Most of the setups were also used for investigations on the fatigue response of FRP bond. Near-end supported single shear tests were carried out by Bizindavyi et al. (2003) and Carloni (2012, 2013). Far-end supported double shear tests by Ferrier (2005) and near end supported double shear tests by Budelmann (2013) and modified beam tests were carried out by Dai (2005). An extensive literature review can be found in Carloni (2013) and Kim and Heffernan (2008).

Bond Stress-Slip Behaviour Under Fatigue Loads

With an increasing number of fatigue cycles, the stiffness of the bond stress-slip response decreases (Bizindavyi et al. 2003; Carloni 2013; Ferrier 2005). This indicates that fatigue damage propagates at the interface between FRP and concrete. The translation in self-similar manner of a certain strain profile along the bond length supports this damage propagation theory such that the point, where the free strain at debonding $\bar{\varepsilon}_{yy}^{fatigue}$ is reached, propagates from the loaded end toward the

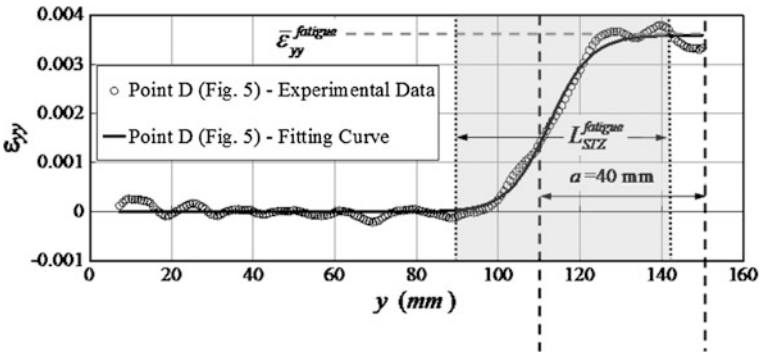

Fig. 6.5 FRP strain profile determined with DIC

other end (see Bizindavyi et al. 2003; Budelmann 2013; Carloni 2013; Ferrier 2005). A similar behaviour was observed by Hankers (1996) at externally bonded steel plates under cyclic loads.

Generally the strain profiles were measured with strain gauges. In Carloni (2013) the strain components were determined on the surface of the FRP and surrounding concrete during fatigue and monotonic tests from the displacement field, which was measured using a full-field optical technique known as digital image correlation (DIC) see (Sutton 1983, 2009).

An example of longitudinal strain distribution along the direction of the fibres determined with DIC is plotted in Fig. 6.5. Details on the strain analysis can be found in Carloni (2012, 2013) and Ali-Ahmad et al. (2006).

The nonlinear strain distribution was approximated by the following function after Ali-Ahmad et al. (2006):

$$\varepsilon_{yy} = \varepsilon_0 + \frac{\alpha}{1 + e^{\frac{y - y_0}{\beta}}} \tag{6.20}$$

where α, β, ε_0, y_0 were determined using nonlinear regression analysis of the computed strains. This approach was previously used for static tests and it can be used for fatigue as well.

The approximated strain distribution along the FRP obtained from Eq. (6.20) is also shown in Fig. 6.5. The stress transfer zone (STZ) can be identified in Fig. 6.5 as the intermediate region where the load is actually transferred from the FRP to the substrate. The length of STZ is the effective length whereas STZ itself is the fracture process zone of the interface. The length of the STZ (L_{STZ}) is termed effective bond length or anchorage length. The constant value of the strain in the fully debonded region was identified as $\bar{\varepsilon}_{yy}$.

From the best-fit strain distribution, the cohesive material law parameter $\tau_{\max}^{fatigue}$ and the fracture parameter $G_F^{fatigue}$ were obtained. In Table 6.1 the average values of the fracture parameters and the value of the strain at debonding $\bar{\varepsilon}_{yy}^{fatigue}$, calculated at

Table 6.1 Fracture parameters during fatigue loading

Test #	$L_{STZ}^{fatigue}$ (mm)	$\bar{\varepsilon}_{yy}^{fatigue}$ ($\mu\varepsilon$)	$\tau_{\max}^{fatigue}$ (N/mm^2)	$G_F^{fatigue}$ (N/mm)	a (mm)	P_{crit}^{Cycles} (N/mm)	g_D (mm)
DS-FT_1 [9]	50	3500	6.0	0.22	0	3.7	0.25
DS-FT_2 [9]	50	4000	6.7	0.27	68	3.6	0.30
DS-FT_3 [9]	56	4100	3.9	0.29	100	3.3	0.50

the peak of ten slow cycles after a certain global slip g_D, measured by two LVDTs, was reached, are reported for three fatigue tests carried out by Carloni and Subramaniam (2013). Ten images, processed with DIC and corresponding to the peaks of the ten slow cycles, were used to calculate the average values reported in Table 6.1. The length of the STZ during fatigue loading $L_{STZ}^{fatigue}$ appeared to be smaller than the one reported in static tests.

Carloni (2013) postulated that the sub-critical crack growth might occur in the epoxy layer rather than in a thin mortar-rich layer of concrete, as typically occurs in monotonic quasi-static tests. A similar observation was found in Carloni (2012) and in Ferrier (2005), in which the authors noticed that the fatigue performances of FRPs were greatly influenced by the physical and mechanical properties of the epoxy. This circumstance was supported by the visual analysis of the FRP sheets after failure. In fact, the debonded surface of the FRP strip was smoother in the first 40 mm close to the loaded end, which approximately corresponded to the length of the cohesive crack a during fatigue (see Carloni 2013).

Carloni (2013) used the relationship of Eq. (6.21) between the load-carrying capacity and the fracture energy of the FRP-concrete interface to prove indirectly that the load at the peak of the ten cycles P_{crit}^{Cycles}, after reaching the slip g_D, was related to the corresponding fracture energy $G_F^{fatigue}$ and, therefore, the approximation of the strain profiles with Eq. (6.20) was acceptable.

$$P_{crit}^{Cycles} = b_l \cdot \sqrt{2 \cdot G_F^{fatigue} \cdot E_f t_f} \tag{6.21}$$

P_{crit}^{Cycles} is provided in Table 6.1 for the three tests and should be compared to the applied load at the peak of the cycles P_{max}, which was equal to 4.2 kN. The calculated loads P_{crit}^{Cycles} were in good agreement with the applied load P_{max}.

Database

From the experimental test data described in Bizindavyi (2003), Budelmann (2013), Carloni (2012), Dai (2005) and Ferrier (2005) the S-N curve can be determined. For determining the number of load cycles N_{30} needed for reaching a debonded length of 30 mm, a linear increase of the debonded length is assumed. The number of load

cycles needed for reaching a decoupled length of 30 mm is calculated for the tests from Bizindavyi (2003), Carloni (2012), Dai (2005) and Ferrier (2005) by linear interpolation using the bond length l_b and the number of load cycles until full decoupling. For the tests from (Budelmann 2013) the number of load cycles is taken from the strain measurements. A decoupling length of 30 mm is reached when the strain measured with the strain gauge A0 or B0 placed 30 mm from the loaded end exceeds the free strain measured with the strain gauge A1 or B1 located in the unbounded region of the CFRP-plate.

For fitting the S-N curve unified related load ranges $S_{0;i}$ at a lower load level of 0 and the corresponding number of load cycles is needed. The unified load range $S_{0;i}$ is determined in a projection analysis using the Goodman relation and Eq. (6.22).

$$S_{0,i} = \frac{\Delta F_{L,0,i}}{F_{Lb}} = \frac{\frac{F_L^O - F_L^U}{F_{Lb}}}{1 - \frac{F_L^U}{F_{Lb}}} = \frac{F_L^O - F_L^U}{F_{Lb} - F_L^U} \tag{6.22}$$

Experimental data from Bizindavyi (2003), Budelmann (2013), Carloni (2012), Dai (2005) and Ferrier (2005) with the calculated number of load cycles N_{30} and the corresponding load range S_0, as well as the width b_L, the thickness t_L, the number of layers n_L and Young's modulus E_L of the tested FRP, can be found in Tables 6.2 and 6.3. Figure 6.6 shows the S-N curve fitted to the experimental data compared with the approach given in the DAfStb-guideline (2012). The load range α is the difference between maximum and minimum load F_L^O–F_L^U related to the monotonic quasi-static load-carrying capacity of the interface F_{Lb}.

A fracture mechanics based method to describe the fatigue behaviour was proposed by Diab (2009) and successively modified by Carloni and Subramaniam (2013).

In Diab (2009) the rate of debonding growth da/dN is related to the interfacial fracture energy:

$$\frac{da}{dN} = m_1 \left(\frac{G_F^{fatigue}}{G_F} \right)^{n_1} \cdot \beta \tag{6.23}$$

The coefficients m_1, n_1 and β can be determined from experimental results. In particular, β takes into account that the crack propagation rate decreases as the debonded region increases. In Eq. (6.23) an additional coefficient, related to the effect of the frequency, was considered equal to 1. $G_F^{fatigue}$ is the interfacial fracture energy during fatigue loading, see Table 6.1. Its relationship with the amplitude and mean value of the load range has not been investigated in the available literature.

Carloni and Subramaniam (2013) modified Diab's formula, as the relationship between the applied load and fracture energy during cycles was indirectly proven:

Table 6.2 Experimental data from Bizindavyi (2003)

Ref.	Test	FRP width b_L (mm)	FRP thickness t_L (mm)	FRP Young's Modulus E_L (N/mm^2)	Number of layers n_L (mm)	Bond length l_b (mm)	Maximum load F_L^O (N)	Minimum load F_L^U (N)	Bond capacity F_{Lb} (N)	Number of load cycles N_{30} (–)	Load range S_0 (–)
Biz.[a]	C1-1a	25.4	0.33	75,700	1	300	8500	0	6480	30	0.76
Biz.[a]	C1-2a	25.4	0.33	75,700	1	300	8500	0	5029	17,323	0.59
Biz.[a]	C1-2b	25.4	0.33	75,700	1	300	8500	0	5029	28,656	0.59
Biz.[a]	C1-3a	25.4	0.33	75,700	1	300	8500	0	4572	21,025	0.54
Biz.[a]	C1-3b	25.4	0.33	75,700	1	300	8500	0	4572	29,790	0.54
Biz.[a]	C1-3c	25.4	0.33	75,700	1	300	8500	0	4572	34,739	0.54
Biz.[a]	C1-3d	25.4	0.33	75,700	1	300	8500	0	4572	67,608	0.54
Biz.[a]	C1-4a	25.4	0.33	75,700	1	300	8500	0	3505	186,222	0.41
Biz.[a]	C1-4b	25.4	0.33	75,700	1	300	8500	0	3505	202,950	0.41
Biz.[a]	C2-1a	50.8	0.33	75,700	1	160	17,000	0	11,135	624	0.66
Biz.[a]	C2-1b	50.8	0.33	75,700	1	160	17,000	0	11,135	788	0.66
Biz.[a]	C2-2a	50.8	0.33	75,700	1	160	17,000	0	9185	6526	0.54
Biz.[a]	C2-2b	50.8	0.33	75,700	1	160	17,000	0	9185	26,832	0.54
Biz.[a]	C2-3a	50.8	0.33	75,700	1	160	17,000	0	7071	34,674	0.42
Biz.[a]	C2-3b	50.8	0.33	75,700	1	160	17,000	0	7071	93,133	0.42
Biz.[a]	C3-1a	50.8	0.33	75,700	1	160	17,000	0	11,460	29	0.67
Biz.[a]	C3-1b	50.8	0.33	75,700	1	160	17,000	0	11,460	60	0.67
Biz.[a]	C3-2a	50.8	0.33	75,700	1	160	17,000	0	9453	113	0.56
Biz.[a]	C3-2b	50.8	0.33	75,700	1	160	17000	0	9453	407	0.56
Biz.[a]	C3-3a	50.8	0.33	75,700	1	160	17,000	0	7453	40,022	0.44

(continued)

Table 6.2 (continued)

Ref.	Test	FRP width b_L (mm)	FRP thickness t_L (mm)	FRP Young's Modulus E_L (N/mm^2)	Number of layers n_L (mm)	Bond length l_b (mm)	Maximum load F_L^O (N)	Minimum load F_L^U (N)	Bond capacity F_{Lb} (N)	Number of load cycles N_{30} (–)	Load range S_0 (–)
Biz.[a]	C3-3b	50.8	0.33	75,700	1	160	17,000	0	7453	40,352	0.44
Biz.[a]	C4-1a	50.8	0.66	75,700	2	300	30,200	0	17496	37	0.58
Biz.[a]	C4-1b	50.8	0.66	75,700	2	300	30,200	0	17496	39	0.58
Biz.[a]	C4-2a	50.8	0.66	75,700	2	300	30,200	0	14402	190	0.48
Biz.[a]	C4-2b	50.8	0.66	75,700	2	300	30,200	0	14402	1062	0.48
Biz.[a]	C4-3a	50.8	0.66	75,700	2	300	30,200	0	11232	7650	0.37
Biz.[a]	C4-3b	50.8	0.66	75,700	2	300	30,200	0	11232	26,687	0.37
Biz.[a]	C5-1a	50.8	0.66	75,700	2	300	30,200	0	18882	38	0.63
Biz.[a]	C5-1b	50.8	0.66	75,700	2	300	30,200	0	18882	97	0.63
Biz.[a]	C4-2a	50.8	0.66	75,700	2	300	30,200	0	16825	195	0.56
Biz.[a]	C5-2b	50.8	0.66	75,700	2	300	30,200	0	16825	1430	0.56
Biz.[a]	C5-3a	50.8	0.66	75,700	2	300	30,200	0	15728	18,682	0.52
Biz.[a]	C5-3b	50.8	0.66	75,700	2	300	30,200	0	15728	31,684	0.52
Biz.[a]	G1-1a	25.4	1	29,200	1	220	11,410	0	6426	5523	0.56
Biz.[a]	G1-1b	25.4	1	29,200	1	220	11,410	0	6426	6830	0.56
Biz.[a]	G1-2a	25.4	1	29200	1	220	11,410	0	4890	8768	0.43
Biz.[a]	G1-2b	25.4	1	29,200	1	220	11,410	0	4890	9627	0.43
Biz.[a]	G1-3a	25.4	1	29,200	1	220	11,410	0	4543	112,227	0.4
Biz.[a]	G1-3b	25.4	1	29,200	1	220	11,410	0	4543	135,273	0.4
Biz.[a]	G2-1a	25.4	1	29,200	1	300	11,410	0	6477	2390	0.57

(continued)

Table 6.2 (continued)

Ref.	Test	FRP width b_L (mm)	FRP thickness t_L (mm)	FRP Young's Modulus E_L (N/mm^2)	Number of layers n_L (mm)	Bond length l_b (mm)	Maximum load F_L^O (N)	Minimum load F_L^U (N)	Bond capacity F_{Lb} (N)	Number of load cycles N_{30} (–)	Load range S_0 (–)
Biz.[a]	G2-1b	25.4	1	29,200	1	300	11,410	0	6477	7832	0.57
Biz.[a]	G2-2a	25.4	1	29,200	1	300	11,410	0	4953	21,714	0.43
Biz.[a]	G2-2b	25.4	1	29,200	1	300	11,410	0	4953	35,949	0.43
Biz.[a]	G2-2c	25.4	1	29,200	1	300	11,410	0	4953	42,308	0.43
Biz.[a]	G2-3a	25.4	1	29,200	1	300	11,410	0	4420	88,609	0.39
Biz.[a]	G2-3b	25.4	1	29,200	1	300	11,410	0	4420	245,893	0.39

[a]Bizindavyi (2003)

Table 6.3 Experimental data from Budelmann (2013), Carloni (2012), Dai (2005) and Ferrier (2005)

Ref.	Test	FRP width b_L (mm)	FRP thickness t_L (mm)	FRP Young's Modulus E_L (N/mm^2)	Number of layers n_L (mm)	Bond length l_b (mm)	Maximum load F_L^O (N)	Minimum load F_L^U (N)	Bond capacity F_{Lb} (N)	Number of load cycles N_{30} (–)	Load range S_0 (–)
Fer.[a]	A 1	16.2	1.38	67,988	1	200	12,072	0	10,284	3	0.86
Fer.[a]	A 2	16.1	1.38	67,476	1	200	11,998	0	10,220	27	0.86
Fer.[a]	A 3	16.2	1.38	67,308	1	200	12,072	0	8942	59	0.75
Fer.[a]	A 4	16.1	1.38	67,160	1	200	11,998	0	8887	118	0.75
Fer.[a]	A 5	16.2	1.38	66,770	1	200	12,072	0	8048	720	0.67
Fer.[a]	A 6	16.2	1.38	66,831	1	200	12,072	0	8048	542	0.67
Fer.[a]	A 7	16.2	1.38	66,312	1	200	12,072	0	7154	6001	0.59
Fer.[a]	A 8	16.2	1.38	66,210	1	200	12,072	0	6707	9653	0.56
Fer.[a]	A 9	16.2	1.38	65,864	1	200	12,072	0	6148	47,948	0.51
Fer.[a]	A 10	16.2	1.38	65,665	1	200	12,072	0	5813	120,251	0.48
Fer.[a]	B 1	12.8	2.57	54,380	1	200	29,113	0	17,797	2425	0.64
Fer.[a]	B 2	12.8	2.9	50,744	1	200	32,851	0	18,968	5210	0.6
Fer.[a]	B 3	12.7	2.65	51,559	1	200	29,785	0	16,222	74,385	0.56
Fer.[a]	B 4	12.7	2.61	48,905	1	200	29,335	0	14,982	207,728	0.53
Fer.[a]	B 5	12.7	2.68	–	1	200	30,122	0	13,342	573,517	0.46
Car.[b]	DS-F1	25	0.167	230,000	1	152	7590	1250	6000	255	0.75
Car.[b]	DS-F2	25	0.167	230,000	1	152	7590	1100	5100	2604	0.61
Car.[b]	DS-F3	25	0.167	230,000	1	152	7590	1100	4500	23,091	0.53
Dai[c]	S1-1	60	0.11	230	1	150	24,600	0	17,958	57	0.73
Dai[c]	S1-2	60	0.11	230	1	150	24,600	0	15,744	4615	0.64

(continued)

Table 6.3 (continued)

Ref.	Test	FRP width b_L (mm)	FRP thickness t_L (mm)	FRP Young's Modulus E_L (N/mm^2)	Number of layers n_L (mm)	Bond length l_b (mm)	Maximum load F_L^O (N)	Minimum load F_L^U (N)	Bond capacity F_{Lb} (N)	Number of load cycles N_{30} (–)	Load range S_0 (–)
Dai[c]	S1-3	60	0.11	230	1	150	24,600	0	12,546	299,162	0.51
Bud[d]	C201	50	1.4	170,000	1	1150	28,382	3820	15,958	127,862	0.49
Bud[d]	C202	50	1.4	170,000	1	1150	28,382	5117	18,005	415,550	0.55
Bud[d]	C203	50	1.4	170,000	1	1150	28,382	5819	16,267	1,634,439	0.46
Bud[d]	C204	50	1.4	170,000	1	1150	30,190	9032	16,267	156,751	0.34
Bud[d]	C205	50	1.4	170,000	1	1150	34,296	15,292	22,562	188,462	0.38
Bud[d]	C206	50	1.4	170,000	1	1150	30,190	21,729	24,942	462,744	0.38
Bud[d]	C207	50	1.4	170,000	1	1150	30,190	22,884	26,204	462,744	0.45
Bud[d]	C208	50	1.4	170,000	1	1150	30,952	5236	20,754	878	0.6
Bud[d]	C209	50	1.4	170,000	1	1150	30,952	10,436	18,374	428,569	0.39
Bud[d]	C2010	50	1.4	170,000	1	1150	30,952	10,175	18,338	428,569	0.39
Bud[d]	C401	50	1.4	170,000	1	1150	24,847	3249	13,768	200,508	0.49
Bud[d]	C402	50	1.4	170,000	1	1150	24,847	11,662	17,576	746,055	0.45
Bud[d]	C403	50	1.4	170,000	1	1150	24,847	13,626	18,862	269,850	0.47
Bud[d]	C501	50	1.4	170,000	1	1150	34,950	25,811	29,798	61,811	0.44
Bud[d]	C502	50	1.4	170,000	1	1150	34,950	25,478	29,560	61,811	0.43
Bud[d]	C503	50	1.4	170,000	1	1150	34,950	5284	16,184	746,055	0.37
Bud[d]	C504	50	1.4	170,000	1	1150	34,950	5986	17,207	269,850	0.39

[a]Ferrier (2005), [b]Carloni (2012), [c]Dai (2005), [d]Budelmann (2013)

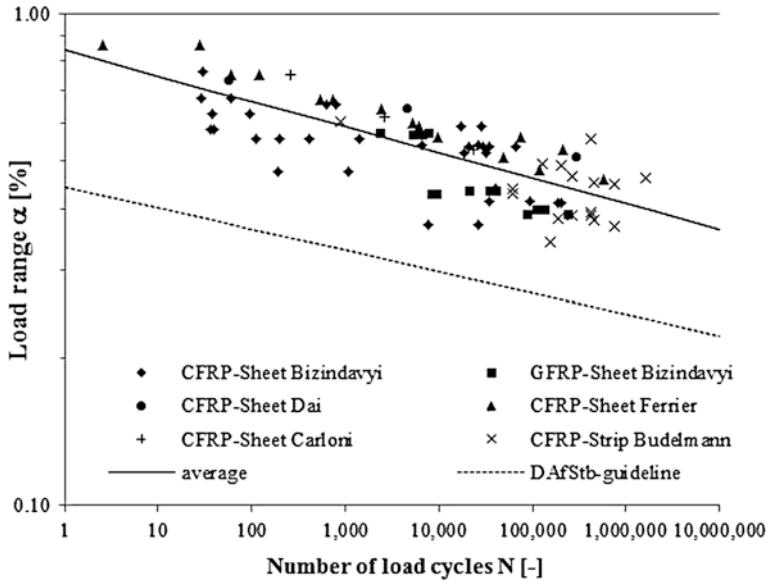

Fig. 6.6 S-N curve and experimental data from Bizindavyi (2003), Budelmann (2013), Carloni (2012), Dai (2005) and Ferrier (2005) in comparison with DAfStb-guideline (2012)

$$\frac{da}{dN} = \bar{m}_1 \left(\frac{\alpha \sqrt{\Delta P \cdot \bar{P}}}{P_{crit}} \right)^{\bar{n}_1} \bar{\beta} \tag{6.24}$$

where $\Delta P = P_{\max} - P_{\min}$ and $\bar{P} = (P_{\max} + P_{\min})/2$ are the amplitude and the mean value of the load range, respectively. P_{crit} is the monotonic quasi-static load-carrying capacity of the interface. The coefficients $\bar{m}_1$, $\bar{n}_1$, $\bar{\beta}$ can be calibrated through the experimental results. α is the frequency coefficient, which takes into account that the fracture properties during fatigue loading depend on the frequency.

With the experimental data and the projection method presented above, another formulation of Eq. (6.24) can be found:

$$\frac{da}{dN} = \frac{1}{N^*} \left(\frac{\left(F_L^O - F_L^U\right)/F_{Lb}}{c \cdot \left(1 - F_L^U/F_{Lb}\right)} \right)^k \tag{6.25}$$

where F_L^O and F_L^U are the maximum and the minimum values of the load range. F_{Lb} is the monotonic quasi-static load-carrying capacity of the interface. The parameters N^*, c and k can be set to 2×10^6, 0.295 and 23.1 using the S-N curve from the DAfStb-guideline (2012) for calculating the crack growth rate in mm per load cycle.

Equation (6.25) neither takes into account that the crack propagation rate decreases as the debonded region increases nor the effect of the frequency. However, it represented an extension of the classical formulation of the Paris' law in which the effect of the amplitude and mean value of the cyclic loading were explicitly considered, see Anderson (2004).

Codes and Guidelines

Most of the existing standards and guidelines consider aspects of fatigue only in a rough way. In all cases the steel stress is limited to avoid a fatigue steel failure and in some cases the FRP strain is limited. A detailed analysis method to avoid intermediate crack debonding under cyclic load only can be found in the DAfStb-guideline (2012). A summary of fatigue aspects in different guidelines can be found in Kim (2008):

ISIS Canada (2001) assumes that fatigue failure of FRP strengthened reinforced concrete beams will occur as a result of fracture of the reinforcing steel and, thus, recommends that the stress levels in the externally bonded FRP be limited such that the steel reinforcing bars do not yield.

fib bulletin 14 (2001) regards the fatigue state of strengthened reinforced concrete beams as a special design consideration. This document recommends that the steel stress range in the fatigue design of CFRP-strengthened beams be restricted to those allowed for an unstrengthened beam.

ACI Committee 440 (2008) gives a creep and fatigue limit for FRP. The magnitude of maximum applied stress including both sustained and repeated loads for CFRP should not exceed 55 % of its ultimate strength.

The Italian code for strengthening existing structures (CNR-DT 200-R1 2004) provides a conversion factor of $\eta_1 = 0.5$ for all types of FRP subjected to fatigue load to account for the potential degradation of FRP-strengthening systems.

The DAfStb-guideline (2012) considers fatigue debonding at the end anchorage of FRPs and between cracks. The steel stress range is restricted after EC2 (EN 1992-1-2 2004) as for an unstrengthened RC structure. The design concept for bond fatigue given in the DAfStb-guideline (2012) is based on the bilinear limit curve of the upper load from Fig. 6.7 and this depends on two verifications. It can be verified whether the load difference ΔF_L^O is within the elastic range $\Delta F_{L;el}$ with Eq. (6.26).

$$\Delta F_{L,el} = 0.348 \cdot f_{ct}^{1/4} \cdot F_{Lb} \geq \Delta F_L^O \tag{6.26}$$

The load difference has to be checked at the end and in the middle part of a strengthened RC structure. In the end part, the load difference ΔF_L^O has to be calculated from the plate end to the first flexure crack. In the middle part the load difference ΔF_L^O between two cracks of a theoretical crack pattern has to be

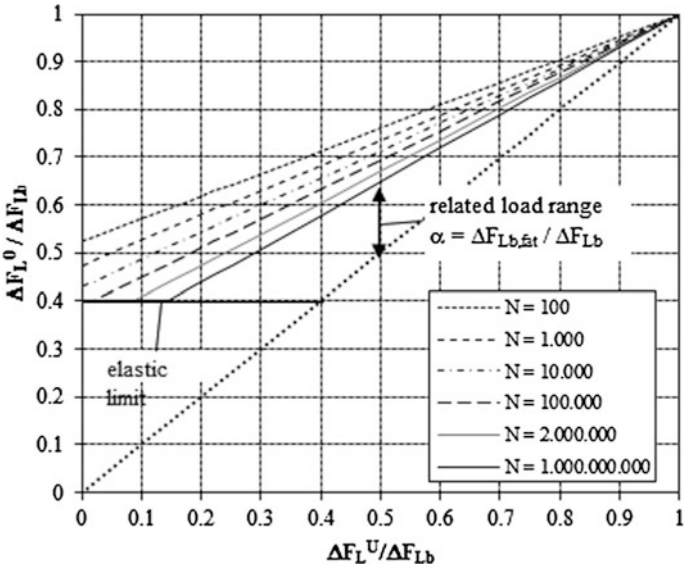

Fig. 6.7 Design concept after DAfStb-guideline (2012)

calculated. For the calculation of the crack spacing and the maximum plate force difference ΔF_{Lb} between cracks the model given in DAfStb-guideline (2012) and German Committee for Structural Concrete (2013) is used. If the condition given by the equation above is not met, the fatigue range $\Delta F_{Lb;fat}$ can be verified as follows:

$$\begin{aligned} \Delta F_{Lb,fat} &= \alpha \cdot \Delta F_{Lb} \geq \Delta F_L^O - \Delta F_L^U, \\ \alpha &= -c \cdot \frac{\Delta F_L^U}{\Delta F_{Lb}} + c, \\ c &= 0.342 \times \frac{N}{N^*}^{-\frac{1}{k}}, \\ N^* &= 2 \times 10^6, \\ k &= \begin{cases} 23.1 \; for \; N < N^* \\ 45.4 \; for \; N \geq N^* \end{cases} \end{aligned} \tag{6.27}$$

The load range between the load difference at the upper load level ΔF_L^O and the lower load level ΔF_L^U has to be smaller than the fatigue range $\Delta F_{Lb;fat}$. The fatigue range $\Delta F_{Lb,fat}$ depends on the lower load level ΔF_L^U and decreases with a rising lower load level ΔF_L^U. It also depends on the number of load cycles N.

The reduction of the fatigue range $\Delta F_{Lb,fat}$ based on an increasing number of load cycles N is described with the factor c given in Eq. (6.27). The Goodman-Smith Diagram shown in Fig. 6.7 illustrates the fatigue design concept. The horizontal line marks the elastic limit calculated with Eq. (6.26). The related

load range α used in Eq. (6.27) and its dependence on the lower load level ΔF_L^U and the number of load cycles N is explained by the linear functions plotted above.

To prevent debonding and damage the limit for the load amplitude has to decrease with an increasing lower load level and an increasing number of load cycles. The design concept after DAfStb-guideline (2012) presented above shows a simple method to calculate the limit for the load amplitude.

Effects of Fire and High Temperature

Introduction

Fire is one of the most serious potential risks for buildings and structures, and for this reason international codes provide specific guidelines to take account of fire in the design of structures (ACI 318-11, EN 1991-1-2, EN 1992-1-2). In some countries (e.g. Italy, Greece, Turkey, Spain, Portugal), the earthquake, which is often follow by fire events, is an event with greater risk for physical injury and damage to objects and properties. However, also in some of these countries, national codes (NTC 2008) have recently introduced more regulation for the fire risk, by considering that human activities are in continuous development and evolution and can be more dangerous than natural events. In this chapter, the main effects of high temperatures on fibre-reinforced composite materials are summarized. In particular, some studies carried out in the last two decades on this topic are cited, mainly to show actual knowledge and future challenge about the degradation of the mechanical properties of FRP materials at high temperatures.

At first, some information about the critical temperatures for FRP are given. Then, some studies related to testing on structural members reinforced with FRP and numerical simulations of the behaviour of FRP materials at high temperatures are mentioned. Although for many applications there is a clear need for protection against high temperatures, the chapter closes with an example that shows how in some cases the protection is already self-provided by non-structural elements having other functions.

Critical Temperatures for the Mechanical Properties

As stated in previous sections, FRP are composite materials successfully applied to repair and/or strengthen RC structures. For external strengthening, the FRP plates are easily bonded on concrete using adhesive, like epoxy resins, which ensure the transfer of forces between concrete and FRP. However, degradation of mechanical properties of composites (strength, stiffness and bond) due to high temperature (Dai et al. 2013; Nigro et al. 2013), moisture absorption (Jia et al. 2005) and cycling

loads (Dai et al. 2005) is a key aspect for a durable efficiency of composite materials.

Concerning high temperature, a critical condition occurs when the glass transition temperature, T_g, of the polymer matrix is achieved, due to the softening of the resin, which reduces the capacity of transfer of forces between the fibres. The precise definition of the value of T_g is still under discussion in the scientific community, because the progressive nature of the softening process makes it difficult to identify a precise temperature limit. Nevertheless, the safety check often is conservatively performed, in the temperature domain, with reference to the value of T_g properly reduced (ACI 440.2R-08 2008).

FRPs which polymerize in ordinary conditions, typical of in situ applications, are characterized by very low T_g (between 45 and 80 °C for normal and heat resistant resins, respectively). For preformed FRPs, used as internal reinforcement, is easily possible to obtain, reinforcements with T_g above 100 °C. Curing processes carried out at temperatures and pressures different from ordinary ones, allow to further increase the T_g.

Although overcoming the T_g implies a reduction in strength of the reinforcement, the drastic degradation of the resistance is reached at temperatures close to melting of the resin (temperature of crystallization, $T_c > T_g$) or even higher. The reduction of stiffness, instead, depends on the type of fibre reinforcement and it is generally negligible compared to the reduction of resistance. Therefore, the real capacity of the concrete members reinforced with FRP reinforcement, at high temperatures, can be considerably high (Nigro et al. 2011a, b, 2013).

Review of Experimental Studies

Recent experimental studies showed that the softening of the resin which begins when T_g is achieved, involves a drastic reduction of the adhesion properties (Bisby et al. 2005). Hence, the efficiency of the strengthening system for existing structures, which mainly depends on the effectiveness of the bond between FRP and concrete, is strongly affected by the temperature.

Some experimental tests (Deuring 1993) showed similar problem when conventional steel strengthening are used without mechanical anchoring. The comparison between steel and FRP strengthening systems showed that FRP, in particular sheets, without protection behave better than steel plates because of the lower heat conductivity and their smaller weight. Clearly, FRP externally strengthened RC beams or slabs need the protection with additional insulation in order to avoid the debonding between FRP sheets or laminates and concrete support. Consequently some researches were devoted to study the performances of FRP strengthened elements protected by different insulation systems in order to individuate the minimum requirements to obtain satisfactory performances in fire (Bisby et al. 2005).

No information is apparently available on the specific mechanical or bond properties of typical FRP systems used for strengthening RC structures after short-term exposure to elevated temperatures, although limited information is available on the residual mechanical properties of specific FRP materials used in the marine, aerospace, and automotive industries after exposure to high temperature (Mouritz and Mathys 1999; Mouritz and Gibson 2006; Bai et al. 2007). Basic research has been reported on the post-heating residual performance of FRP wrapped concrete cylinders (Cleary et al. 2003; Saafi and Romine 2002), although the data presented in these studies do not elucidate the specific performance of the FRP systems. Only one limited study is available on the high temperature performance of the FRP-to-concrete bond loaded in shear (Gamage et al. 2005), although residual properties are not addressed. Several large-scale standard fire tests have also been performed (Deuring 1993; Blontrock et al. 2001; Kodur et al. 2007), but the data do not address the specific performance of the FRPs either during or after high-temperature exposure.

A significant research effort over the past decade has demonstrated that appropriately designed and adequately insulated FRP strengthened RC beams, slabs, and columns, are capable of achieving adequate fire endurances (Kodur et al. 2007). However, these researches have not provided much insight into the specific performance of the FRP strengthening systems or the bond between the FRP systems and the substrate concrete, either during exposure (i.e., at high temperature) or once they have cooled to room temperature (i.e., residual performance). Information is thus required before defensible strengthening limits and allowable thermal exposures can be suggested for FRP strengthening systems, particularly in cases where the FRP system is required to be effective during or after a fire (Porter and Harries 2005). Information is also needed to develop economical fire insulation schemes for FRP strengthened members, even in cases where the FRP is not required to be structurally effective during a fire.

Numerical Modeling

Probably, in order to extend the results of experimental tests to different cases, using a numerical model could be appropriate. Indeed, the behaviour of structures exposed to fire is usually described in terms of fire resistance but, in real buildings, structural members are part of a continuous assembly, and building fires often remain localized, since the fire affected region of the structure receiving significant restraint from cooler areas surrounding it. The real behaviour of these structural elements can therefore be very different from that indicated by standard furnace tests and should be investigated, as is usual within the Fire Safety Engineering approach.

Clearly, the accuracy of the thermo-mechanical analysis is dependent on the main properties required to calculate the temperature distribution (i.e. specific heat, thermal expansion and thermal conductivity) and the constitutive laws used to

define the mechanical behaviour of materials (i.e. strength, stiffness and bond properties), both at ambient and elevated temperatures. For many of these parameters suggestions in technical code are not univocal for concrete and are still lacking for FRP. Thus, more research is needed to improve the accuracy of the numerical models.

Obviously, if the FRP strengthening is not directly heated by fire or other sources of heat, the performances may be better. Hence, FRPs can be successfully used to strengthen bridges, where fire is not a primary action to be considered during design (Bisby et al. 2005). Nevertheless, it should be noted that bituminous paving casting on a bridge deck can easily lead to have high temperature (e.g. 200 °C).

On this issue Nigro et al. (2013a, b) investigated the thermo-mechanical behaviour of RC bridge decks strengthened with externally bonded FRP plates. The results are summarized in the following section.

The Effects of High Temperatures in a Practical Application

In Nigro et al. (2013a, b) two possible environmental conditions leading to thermal states different from the normal ones were studied with reference to bridge decks: (a) fire exposure over the bridge deck due to an accident involving camions; (b) bituminous paving casting on a bridge deck. Indeed, in both case the temperature at the FRP-to-concrete interface can overcome the above mentioned glass transition temperature, T_g.

The relationships suggested by Italian and American codes, to evaluate the limit strain for FRP debonding at normal temperature, were modified to take into account the effect of high temperature on the debonding of FRP. Then, thermo-mechanical analyses were performed by varying the thicknesses of the slab and the protection layer in order to assess their influence on the thermal field in the structural member. Furthermore, normal resin (NR) with T_g = 45 °C and heat-resistant resin (HR) with T_g = 80 °C were considered. The results were discussed in terms of both temperatures and safety checks carried out for both ultimate and serviceability limit states (ULS and SLS).

The ULS checks were always satisfied, mainly because the flexural capacity provided by FRP can be neglected during fire or maintenance activity. By contrast, the SLS checks performed to assess the damage levels in the FRP strengthening system during these events show that constructive details and type of resin play a key role.

In the case of fire event over the bridge deck, if the strengthening is on the bottom side, for typical design load level η_{fi} = 0.7, FRP damages (i.e. debonding) were not attained for long time of fire exposure, even if the resin achieved the glass transition temperature, T_g. If the strengthening is located on the top side of the slab, the use of heat resistant (HR) resins is suggested. If normal resin (NR) is used, a protection layer on the FRP strengthening is recommended, in order to increase the maximum time of fire exposure without FRP damage.

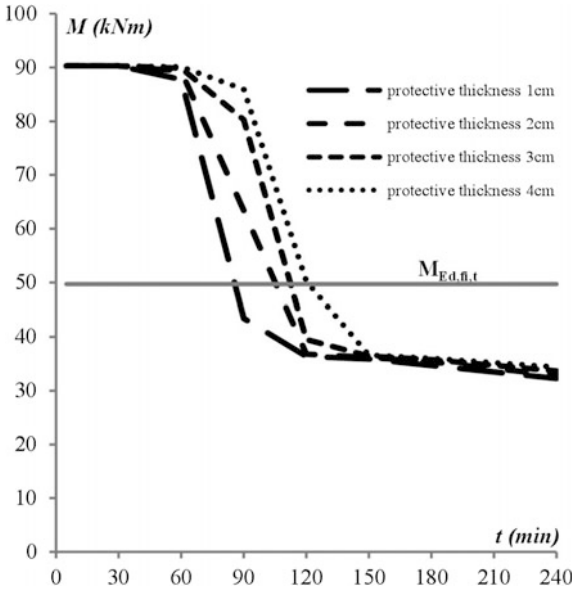

Fig. 6.8 Slab safety check in hogging moment region (fire on the bridge)—T_e = 25 °C—Slab thickness = 15 cm—(NR)

In order to show that the achievement of the T_g may be not a critical condition for the strengthening system, in Fig. 6.8 the bending moment of the FRP strengthened slab, $M_{Rd,fi,FRP}$, reduced for the effect of the fire exposure, is plotted versus the time for the 15 cm thick slab, normal resin and four thicknesses of protective layer, t_{prot}. Moreover the bending moment in fire situation $M_{Ed,fi}$ = 49.7 kNm is shown. Note that $M_{Rd,fi,FRP}$ was calculated by using the relationships suggested by CNR DT 200/2004 to evaluate the debonding strain at ambient temperature. As stated above, the relationships were modified to take into account the effect of high temperature.

Figure 6.8 shows that the time of fire exposure before the debonding of the FRP ranges between 82 and 120 min. Note that these values are higher than those related to the achievement of the T_g at the FRP-to-concrete interface (i.e. 50 and 80 min) and probably more realistic to assess the FRP damage.

In the case of bituminous paving realization, for strengthening on the bottom side, the results are quite similar to those obtained in case of fire. On the other hand, if the strengthening is located on the top side of the slab, the use of HR resins is necessary in order to avoid damages in the FRP strengthening. Otherwise thick protective layer of concrete is required also for low load levels.

The results obtained through the relationships provided by different codes (i.e. Italian and American codes) for ambient temperature and refined with the suggested model are in a good agreement (see Fig. 6.9). However, so far, more research is needed to improve the reliability of codes suggestion.

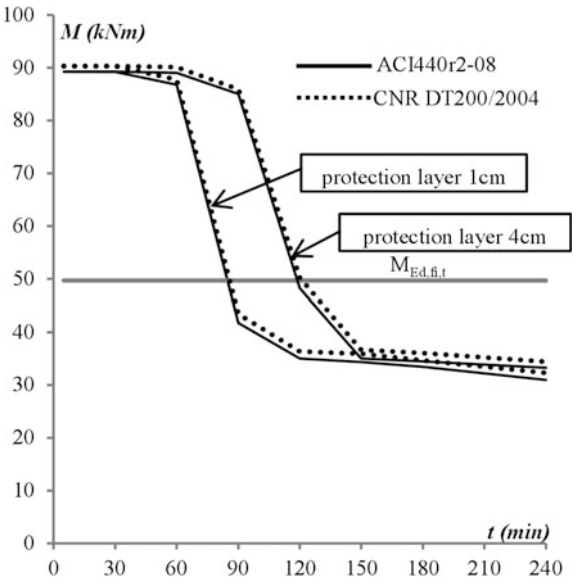

Fig. 6.9 Comparison between codes

Long Term Properties of FRP Systems

Introduction

Regarding the long term performance of a composite system, few authors have dedicated their efforts to the assessment of the performance of the intervening materials (Diab and Wu 2007; Wu and Diab 2007; Meaud et al. 2011).

Apart from changes in applied external actions, the long term performance of a CFRP-adhesive-concrete system is only expected to be affected by the creep, shrinkage or relaxation of each of the components of the system. While the creep and shrinkage of concrete have already been comprehensively studied over the years, limited information is available regarding the creep/shrinkage/relaxation of composite materials. In this chapter a resume on the collected information in this respect is provided.

FRP Relaxation

Bibliographic research has shown that FRPs are known to present low pre-stress losses, as a result of their relatively low elastic modulus (Lopez-Anido and Naike 2000), and lower stress relaxation than steel strands (Dolan et al. 2001; Sayed-Ahmed 2002). In fact, even though FRP materials are able of exhibiting an

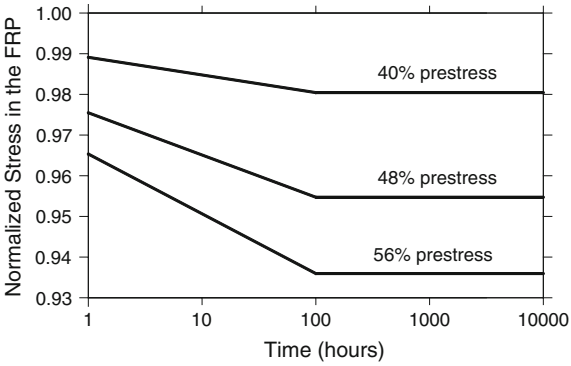

Fig. 6.10 Stress relaxation in CFRP sheets. Adapted from Wang et al. (2012)

elastic modulus, E_f, close to 200 GPa, most of the materials available reveal to have an average maximum E_f of about 160 GPa.

Wang et al. (2012) carried out relaxation tests in CFRP sheets and concluded that the relaxation loss due to sustained deformation levels ranging between 40 and 56 % of the material's tensile strength was determined to be 2.2–6.6 %, as demonstrated in Fig. 6.10. Moreover, this relaxation was mostly concentrated in the first 100 h of sustained deformation, as depicted in Fig. 6.10 and, after this period it becomes almost negligible. These authors have even suggested that the measured relaxation is primarily caused by the relaxation of the resin and straightening of fibres. The carbon fibres themselves are identified as having no relaxation whatsoever (Dolan et al. 2001).

According to Dolan et al. (2001) the relaxation losses in FRP tendons can be caused by three main sources: the relaxation of resin that bonds the fibres together, the lack of parallelism between individual fibres, and the relaxation of fibre itself. Due to these reasons, the relaxation is a characteristic attributable to the fibre type and is generally lower than 12 % over the life of the structure. In the case of CFRP tendons, relaxation losses of approximately 5 % are reported.

Based on these assumptions, it is suggested that FRP relaxation is not a relevant effect for the long-term performance of CFRP laminates. Since in FRP laminates the fibre content is particularly large when compared to FRP sheet coupons, the matrix bonding them together will take only a small portion of the applied load and, therefore, the first source of relaxation may be ignored. Regarding the alignment of the fibres, since FRP laminates are produced by machines, in opposition to FRP sheets, which are manually applied, no significant eccentricities are expected along each fibre and as a result, the second source of relaxation may also be disregarded. Finally, as carbon fibres themselves are reported to have no relaxation, the total amount of relaxation expected is even more reduced.

Adhesive Shrinkage

The volumetric shrinkage of epoxy-based adhesives is generally restricted to the shrinkage occurred during the curing process and is found to be within the range 2–7 % (Li et al. 2004; Yu et al. 2005; Khoun and Hubert 2010).

Concerning the epoxy-based adhesives used in structural applications they reveal such an insignificant shrinkage coefficient, that this parameter is often not even quantified in most materials' datasheets. However, when complete cure is achieved, the shrinkage coefficient variation becomes negligible, as suggested by (Yu et al. 2005; Khoun and Hubert 2010), and the long-term behaviour of the adhesive is no longer shrinkage dependent, but creep-dependent as it will be revealed hereafter.

Adhesive Creep

Introduction

The creep behaviour of plastics is usually fragmented in three major creep stages (ASTM 2990 2001, Majda and Skrodzewicz 2009): primary creep, secondary creep and tertiary creep. As depicted in Fig. 6.11, in the first phase the material adjusts its deformation level to the installed level of stress. This phase is followed by a stationary stage where creep gradually increases until a third phase is reached, where strain suddenly increases and fracture occurs. It is believed that this behaviour is valid under any applied stress, temperature and humidity. However, for low levels of applied stress, the time necessary to reach the tertiary creep state may be so long that it may never be achieved.

The primary function of an adhesive in structural applications is to transmit stress equally over large areas without loss of integrity (Feng et al. 2005). Structural adhesives exhibit, however, notable viscoelastic behaviour, since their deformation, ε, under a constant stress, σ, varies significantly in time. This behaviour is frequently modelled using rheological models and is usually illustrated by means of Hookean springs and Newtonian dashpots that replicate, respectively, the elastic

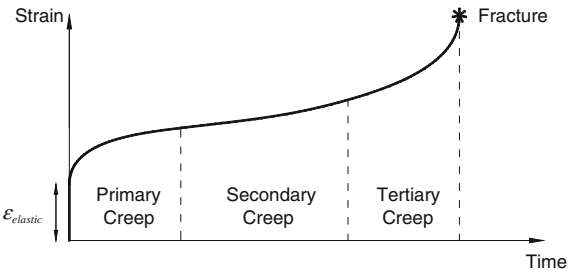

Fig. 6.11 The three stages of creep (at constant stress, temperature and humidity)

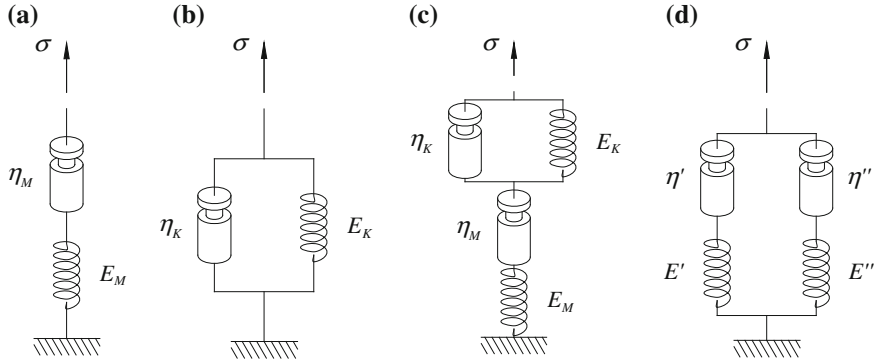

Fig. 6.12 **a** Maxwell model, **b** Kelvin model, **c** Burgers model—common configuration, **d** Burgers model—alternative configuration

and viscous components of the material's behaviour (Brinson and Brinson 2008). In Fig. 6.12, the most common rheological models are presented:

- Maxwell Model—illustrated in Fig. 6.12a, this model is a 2-parameter model that results of associating, in series, a spring with E_M elasticity and a dashpot characterized by η_M dynamic viscosity;
- Kelvin Model—depicted in Fig. 6.12b, it is also a 2-parameter model that consists in combining, in parallel, a spring of elasticity E_K and a dashpot of η_K dynamic viscosity;
- Burgers Model—schematized in Fig. 6.12a–d, this 4-parameter model can be obtained by joining in series Maxwell and Kelvin's Model (E_M, η_M, E_K and η_K in Fig. 6.12c or, in alternative, by connecting two Maxwell models in parallel (E', η', E'' and η'' in Fig. 6.12d).

It is possible to create models like the generalized Maxwell Model or generalized Kelvin Model, depicted in Figs. 6.13 and 6.14 (Brinson and Brinson 2008).

It is relatively simple to obtain the solution of each of these models and, the deduction of each equation can be found in Costa and Barros (2011).

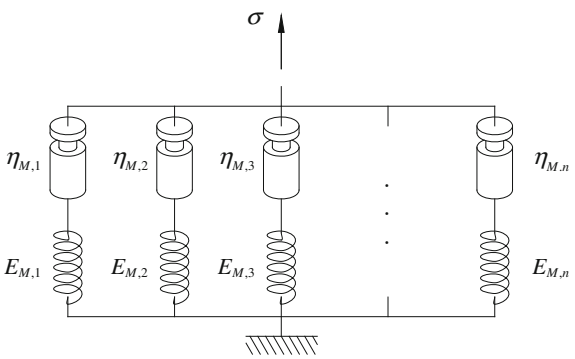

Fig. 6.13 Generalized Maxwell fluid

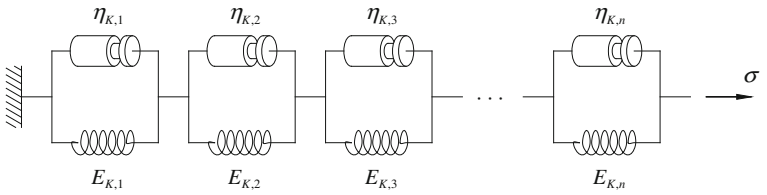

Fig. 6.14 Generalized Kelvin solid

Standards on Creep Behaviour

According to ISO 899-1 (2003) test method, load shall be applied smoothly to a standard specimen, as defined in ISO 527-2 (1993), within 1–5 s and maintained for at least 1000 h (approximately 42 days). Strains, temperature and humidity should be measured according to the schedule presented in Fig. 6.15.

ISO 527-2 (1993) recommends bone-shape specimens to be moulded using the geometry depicted in Fig. 6.16 (see also Table 6.4).

For different temperature and/or humidity level, one creep curve shall be obtained. To construct the desired creep curves, creep strains and/or creep moduli (defined in Eq. 6.28) are plotted against the logarithm of time, for every initial level of applied stress, σ, (see Fig. 6.17). Isochronous curves, which consist in Cartesian plots of stress versus strain at specific time instants, similar to those depicted on Fig. 6.17c, can also be presented.

$$E_e = 2G_r(1 + \nu) \tag{6.28}$$

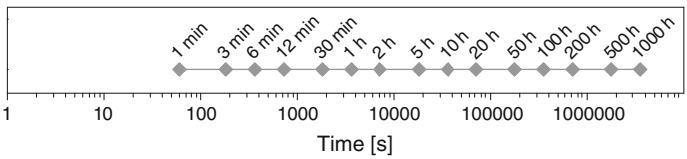

Fig. 6.15 Data acquisition schedule (ISO 899-1 2003)

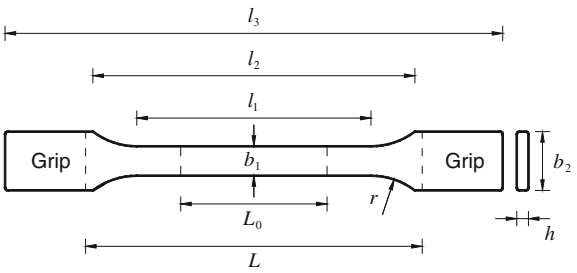

Fig. 6.16 Directly-moulded specimens (Type 1A, ISO 527-2 1993)

Table 6.4 Dimensions, in millimetres, of ISO 527-2 (1993) directly-moulded specimens (Type 1A)

Variable	Description	Dimension (mm)	Tolerance (mm)
b_1	Width of the narrow portion	10	±0.2
b_2	Width at the ends	20	±0.2
h	Preferred thickness	4	±0.2
L	Initial free distance between grips	115	±1
L_0	Gauge length	50	±0.5
l_1	Length of the narrow parallel-sided portion	80	±2
l_2	Distance between broad parallel-sided portions	104–113	–
l_3	Overall length	≥150	–
r	Radius	20–25	–

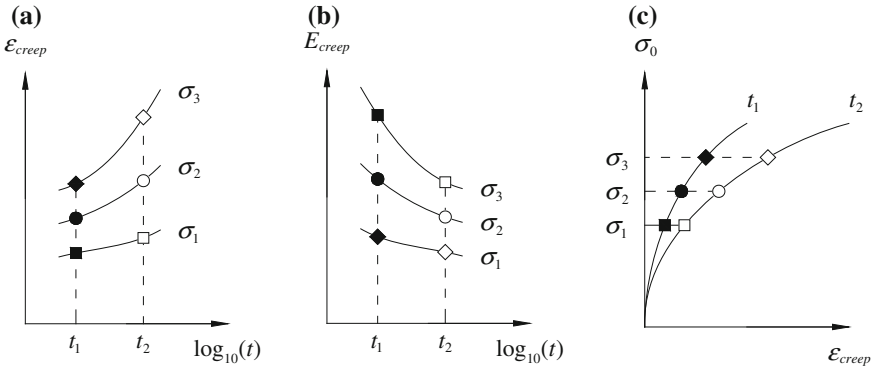

Fig. 6.17 Example of creep curves (ISO 899-1 2003): **a** creep strain curves, **b** creep modulus curves and **c** isochronous stress–strain curves

ASTM 2990 (2001) also addresses creep of plastic materials under specified environmental conditions. Loading shall also be applied in the specimen rapid and smoothly in 1–5 s, and the strains shall be recorded at the time instants shown in Fig. 6.18. To evaluate creep, the use of the normalized specimens produced according to ASTM D 638 (2003) is suggested (Fig. 6.19; Table 6.5).

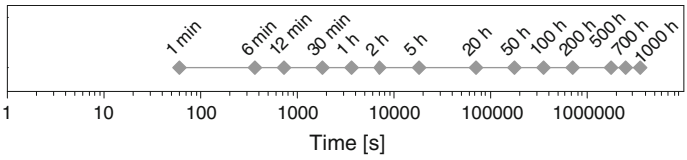

Fig. 6.18 Strain measurement schedule (ASTM 2990 2001)

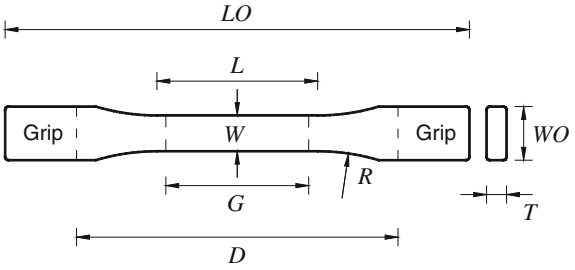

Fig. 6.19 Directly-moulded specimens (Type 1A, ISO 527-2 1993)

Table 6.5 Dimensions, in millimetres, of ASTM D 638 (2003) preferred specimens (Type I)

Variable	Description	Dimension (mm)	Tolerance (mm)
D	Distance between grips	115	±5
G	Gauge length	50	±0.25
L	Length of narrow section	50	±0.5
LO	Overall length	≥165	–
R	Radius of fillet	76	±1
T	Thickness	≤7	–
W	Width of narrow section	19	+6.4
WO	Width at the extremities	80	±2

Research on Creep Behaviour

Feng et al. (2005) suggested that it is possible to estimate the tensile creep strain, $\varepsilon_{creep}(t,T)$, by the exponential function:

$$\varepsilon(t,T) = \frac{\sigma_0}{E_0} + \sigma_0\left(\frac{1}{E_e} - \frac{1}{E_0}\right)\left(1 - e^{-(t/t^*)^{1-n}}\right) \tag{6.29}$$

where σ_0 is the applied stress level, E_0 the initial Young modulus, E_e is the equilibrium modulus given in Eq. (6.28), t^* is the relaxation time and n a coupling parameter related to moisture absorption.

$$E_e = 2G_r(1+\nu) \tag{6.30}$$

where G_r is the rubbery plateau shear modulus, and ν the Poisson's ratio ($\nu = 0.5$ since the material is in the rubbery state). Feng et al. (2005) obtained in their tests values of n ranging from 0.51 to 0.73. Majda and Skrodzewicz (2009) proposed a model purely based on Burgers Model:

$$\varepsilon(t,T) = \frac{\sigma_0}{E_0} + \frac{\sigma_0}{\eta_0}t + \frac{\sigma_0}{E_1}\left(1 - e^{-t/t^*}\right) \tag{6.31}$$

where

$$t^* = \frac{\eta_1}{E_1} \tag{6.32}$$

Majda and Skrodzewicz (2009) also suggested that the coefficients of dynamic viscosity, η_0 and η_1, as well as the elastic modulus are primarily dependent on the applied stress, and:

$$\eta_0(\sigma_0) = e^{a_1 - a_2\sigma_0} \tag{6.33}$$

$$\eta_1(\sigma_0) = e^{a_3 - a_4\sigma_0} \tag{6.34}$$

$$E_1(\sigma_0) = a_5\sigma_0^2 - a_6\sigma_0 + a_7 \tag{6.35}$$

The rheological properties (E_0, E_1, η_0 and η_1) were quantified by means of nonlinear regression analysis of the experimental creep tests at four different levels of applied stress, at a constant temperature of 22 °C (Table 6.6). Later, the different a_i coefficients can be obtained applying ordinary trend lines (logarithmic/quadratic regressions) as well as by non-linear regression (Table 6.7).

Choi et al. (2007) presents the results of creep tests performed in double-shear specimens during 6 months, where creep specimens with different adhesive layer thickness and applied stress were considered. The authors suggest that the total strain due creep also follows the following exponential law:

$$\varepsilon(t,T) = \frac{\sigma_0}{E_0} + \sigma_0\frac{\phi_u(t_\infty)}{E_0}\left[1 - e^{-t/t^*}\right] \tag{6.36}$$

with the values for the parameters indicated in Table 6.8.

By carrying out tensile tests with a current type of adhesive used to bond CFRP laminates to concrete in the NSM technique, Costa and Barros (2013) and Costa (2014) have concluded that after 2 days of curing, the properties of the adhesive are nearly the same as obtained for the recommended curing time (7 days).

Table 6.6 Parameters of the Burger's model determined on creep test of an epoxy adhesive at 22 °C (Majda and Skrodzewicz 2009)

σ_0 (MPa)	E_0 (GPa)	η_0 (GPa h)	E_1 (GPa)	η_1 (GPa h)	t^* (min)
15	2.232	22.4	1.173	0.48	24
20	2.232	4.12	0.788	0.23	18
25	2.232	1.49	0.896	0.07	5
30	2.232	0.36	1.380	0.06	3

Obs. The tensile strength of the adhesive is 46.6 MPa

Table 6.7 Values of a_i for simple and non-linear regressions (Majda and Skrodzewicz 2009)

Coefficient	Unit	Trend line	Nonlinear regression
a_1	ln(Pa s)	35.8	37.38
a_2	Pa-1 ln(Pa s)	27×10^{-8}	31.97×10^{-8}
a_3	ln(Pa s)	30.3	30.72
a_4	Pa^{-1} ln(Pa s)	14×10^{-8}	16.62×10^{-8}
a_5	Pa^{-1}	9×10^{-6}	12.27×10^{-6}
a_6	–	394	516.9
a_7	Pa	50.2×10^{8}	60.70×10^{8}

Table 6.8 Test results in laboratory environment −20 °C and 50 % relative humidity (Choi et al. 2007)

Specimen	Epoxy thickness (mm)	σ_0 (MPa)	Monitored FRP	$\phi_u(t_\infty)$	t^* (days)
1	0.242	0.09	Face 1	1.17	43.3
			Face 2	1.02	2.1
2	0.176	0.17	Face 1	2.89	1.1
			Face 2	2.94	1.7
3	1.500	0.17	Face 1	2.59	0.2
			Face 2	2.39	0.1

Double-shear specimen ultimate resistance: 0.56 MPa

By performing creep tensile tests with three series of specimens of this type of adhesive, these authors have verified that up to sustained stress levels of 60 % of the adhesive's tensile strength, the adhesive behaves as a classic visco-elastic material and can easily be parameterized using the modified Burgers model (Figs. 6.20, 6.21 and 6.22; Table 6.9). In the experimental tests performed, the results suggest that the properties of the adhesive tend to deteriorate with time and therefore, a special attention should be taken regarding the time between adhesive production and

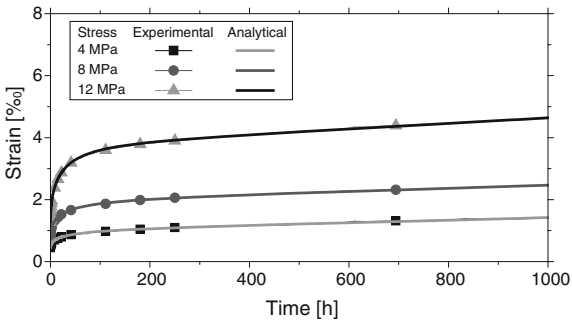

Fig. 6.20 Modified Burgers model—Series I

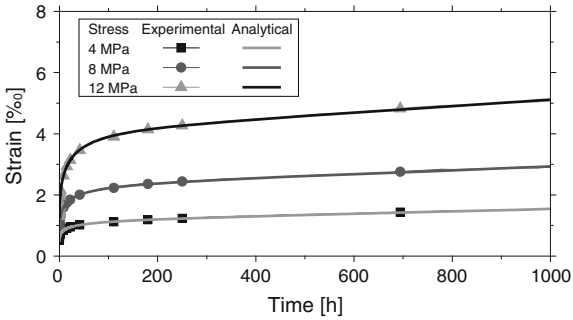

Fig. 6.21 Modified Burgers model—Series II

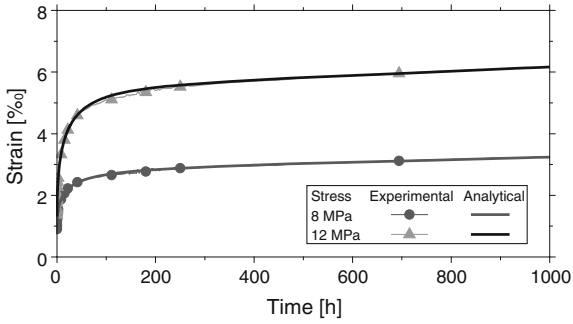

Fig. 6.22 Modified Burgers model—Series III

application. It is also noteworthy that after 1000 h of loading, the adhesive samples exhibited about 4 times the deformation at time of loading (creep modulus of roughly 25 % of the initial stiffness) without rupturing. According to the initial tensile tests performed, a maximum strain at rupture of about 3 ‰ was obtained, while during the creep tests the material was able of somehow reorganizing its internal structure to withstand almost the double of this deformation.

Based on the experimental results the following equation was proposed to estimate the tensile creep modulus (Costa and Barros 2013):

$$E_{creep}(t) = \frac{\sigma}{\varepsilon_{creep}(t)} = E_{creep} = \frac{1}{{}^{1}/_{E_M} + {}^{t}/_{\eta_M} + {}^{1}/_{E_K}\left(1 - e^{-\left(\frac{E_K}{\eta_K}t\right)^{1-n}}\right)} \quad (6.37)$$

where its good predictive performance is visible in Fig. 6.23 by considering the data from Table 6.9.

Table 6.9 Average modified Burgers equation parameters of all series tested

Parameter	E_M (GPa)	η_M (GPa h)	E_K (GPa)	t^* (h)	η_K (GPa h)	n
Series I	9.49	13,482	5.27	24.3	128	0.47
Series II	8.80	11,544	4.50	19.7	88.7	0.53
Series III	8.84	18,446	3.09	18.8	58.1	0.50
Average	9.04 (0.39) {4 %}	14,491 (3560) {25 %}	4.29 (1.10) {26 %}	20.9 (3.0) {14 %}	91.7 (35.2) {38 %}	0.50 (0.03) {6 %}

Average (Standard Deviation) {Coefficient of Variation}

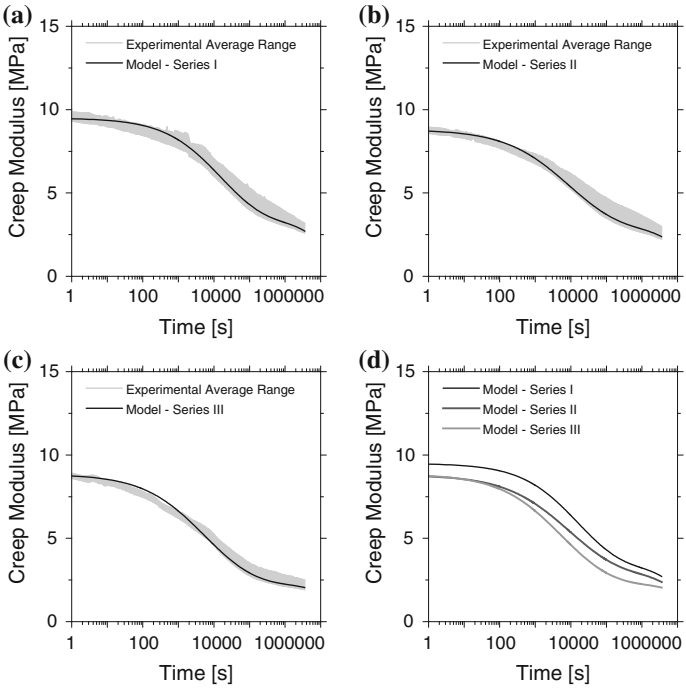

Fig. 6.23 Creep modulus curves based on the analytical results: **a** series I, **b** series II, **c** series III and **d** all analytical curves (Costa 2014)

Anchorage Systems for External Strengthening with FRP

Special Anchorage for Flexural Strengthening

For flexural strengthening the most common anchorage system is given by a FRP sheet or a FRP or steel laminate glued transversally to the strengthening direction. The good performance of such a type of anchoring was tested in Ceroni et al. (2008)

Fig. 6.24 Possible shear U-shaped anchoring devices (Ceroni 2010)

on specific bond tests. This is a reliable solution when the FRP-to-concrete width ratio is less than 1, because the transversal sheet/laminate allows extending the width of concrete covered by the FRP strengthening. In Ceroni and Pecce (2010) a simple method based on geometrical considerations is proposed in order to take into account such an enlargement of the bonded width in the theoretical expression of the debonding load.

When the FRP-to-concrete width ratio approaches to 1, a simple transversal strip becomes unhelpful and U-shaped fibre sheets result more efficient. For example one strip at the end or strips distributed along the beam can be considered (see Fig. 6.24): relevant increasing of the ultimate strength and ductility at failure can be obtained by using these systems (Ceroni 2010) allowing a better use of the tensile strength of the fibres. Sharp edges of the section are recommended to be mechanically rounded before application. In this case, a minimum radius of 30 mm is recommended.

In Al-Mahaidi and Kalfat (2011) the efficiency as anchor devices of unidirectional CFRP fabric wrap applied orthogonally or parallel to the direction of the FRP reinforcement was tested by means of bond tests. In the former configuration the load increase was of 19–28 % mainly due to a strut-tie resistant mechanism resulting from the fabric fibres inclining towards the load direction; in the latter configuration the load increase was 18–37 % due to a transfer of bond stresses to a greater distance from the loaded end.

Steel U-shaped devices as the ones tested by Blaschko (2001) and Mukhopadhyaya et al. (1998) can be an alternative solution for end anchorage. The basic scheme of tests made with special anchoring devices for CFRP strips is shown

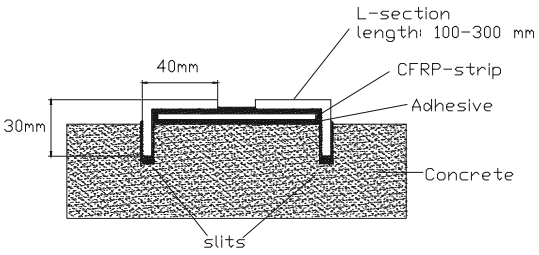

Fig. 6.25 Anchorage for CFRP strips special anchorage system (Zehetmaier 2000)

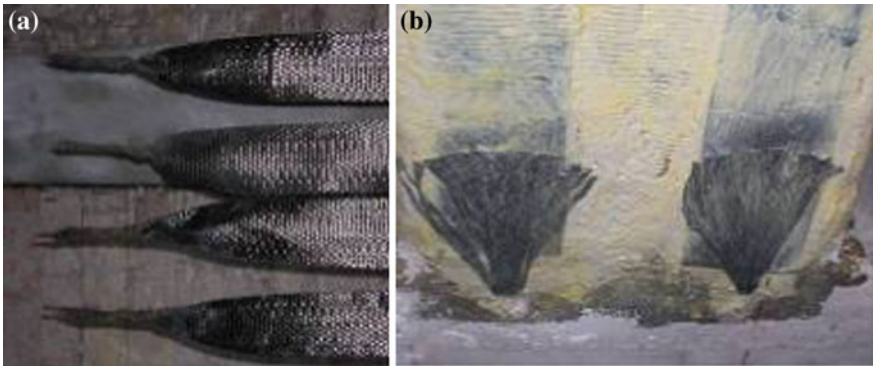

Fig. 6.26 **a** Carbon fibre fan anchor; **b** splaying of fibres outwards the hole

in Fig. 6.25 (Zehetmaier 2000). This system can be applied in case of strengthening of slabs, where no wrapping is possible, or local strengthening and as an anchorage for pre-stressed strips. A minimum concrete cover of about 20 mm is required.

In general, anchoring devices that may influence the integrity of the strengthening system should be avoided. For example, anchoring solution with bolts need of holes that could lead to interlaminar shear failure or splitting of the strip. Moreover, holes reduce the cross section of the strip. However, in case of using bolted systems, it is not adequate to drill through the strengthening strip omitting special provisions, as compressive forces can weaken the strip. Multidirectional fibres at the location of the bolts can be used in order to allow the end tabs take the full force to be anchored (Tan 2001). Bolts should be anchored in the concrete to a depth beyond the steel reinforcement.

Bolted devices could give a better performance if used to anchor prefab laminates with suitable systems provided by manufacturers.

Nail anchors made by wide ringed head nylon anchor with zinc plated hammer screw were used by (Prota et al. 2006) to mechanically anchor beams strengthened with steel tape and cementitious grout.

Fibre fan anchor systems (see Fig. 6.26) are becoming very diffuse. A hole is drilled in the concrete on the same plane of the strengthening. A glass or carbon fibres tow (see Fig. 6.26a) is forced through the impregnated fabric end into the predrilled hole and the ends are splayed outwards on the continuous sheet reinforcement with epoxy resin (see Fig. 6.26b).

Experimental studies about the effectiveness of fan shaped anchors were made by (Özdemir 2005); he founded that: (1) anchors have to be inserted at least 50 mm into the core of the concrete (depth of 130–150 mm); (2) the cross-sectional area of anchor has to be at least two times greater than the cross-sectional area of the longitudinal sheet; (3) splitting the anchor into as many smaller anchors at about a 40 mm spacing as possible.

Such type of anchoring system was tested also by (Ceroni and Pecce 2010) that achieved an increasing of ultimate strength at least of 25 % in bond tests on

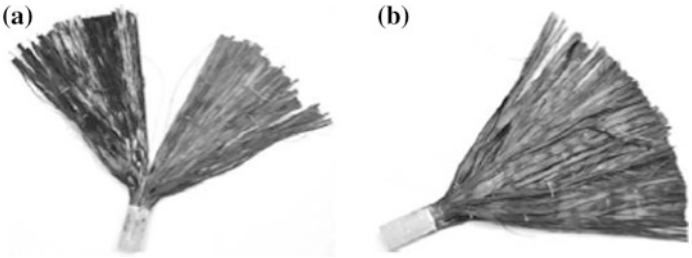

Fig. 6.27 **a** Bow-tie anchor, **b** single fan anchor (Zhang and Smith 2012a)

concrete blocks externally strengthened with carbon sheets when carbon FRP fans were used as end anchoring devices. It is worth to note that the details and accuracy of application procedures can be very influential on the strength increase.

Also (Orton et al. 2008) focused attention on the constructive detailing requested during the installation phase for warrant the efficiency of fan shaped anchor systems.

The effects of anchor splay diameter, anchor diameter and thickness of the FRP sheet have been investigated in (Niemitz et al. 2010).

In Eshwar et al. (2008) the effect of the location and the embedment of spike anchors (10 mm diameter) was experimentally investigated; the experimental results evidenced a significant improvement of strength (25–200 %). A minimum embedment depth of 50 mm in the concrete substrate is suggested, since further increase of the depth resulted ineffective. Multiple anchor spikes significantly increase the strength (+200 %).

In Zhang and Smith (2012a) the influence of FRP anchor fan configuration and dowel angle on the effectiveness of such an anchoring system for FRP reinforcement was investigated in several shear bond tests. In particular, bow-tie FRP anchors (fans oriented in opposite direction along the longitudinal FRP reinforcement) and single fan FRP anchors (fan fibres oriented only in one direction) were tested (see Fig. 6.27). Tests evidenced that single fan FRP anchors with the fan oriented in the direction of load allowed an increasing of the failure load of about 100 % compared with the not anchored specimens. The same load increase was attained using the bow-tie FRP anchors, although the fibre content was twice in this case. When the single fan anchor is positioned with the fan in the reverse direction of the applied load the efficiency into increase the failure load was lower (+60 %). Moreover, the load-slip experimental curves evidenced that the FRP fan anchors enabled a friction resistance that gave to the joint a post-peak reserve and larger ultimate slip, especially in the case of bow-tie configuration. For the single fan anchor the increasing of the angle of the anchor dowel (in the range 45°–157°, while in the basic configuration the angle is 90°) respect to the led to an increase of the failure load (25–160 %) and a decrease of the ductility of the joint due to the brittle failure of the anchor.

In Zhang and Smith (2012b) multiple single fan anchors (one, two, three) were tested in bond tests that substantially evidenced higher maximum load as the number of fan increase, even if the results were more scattered, and lower maximum slip. The concept of flexible and rigid anchors was also introduced and tested: in the flexible anchor there is no epoxy impregnating the region where the fibres of the anchor bend 90° at the junction of the fan and dowel components in order to provide larger slippage of the reinforcement. Experimental results evidenced that in the rigid anchored joints, after the plate debonding, the anchors failed immediately and no post-peak reserve of strength was observed with a consequent reduction of maximum slip that was on average only 36 % of the value attained in the flexible anchored joints. The maximum load in the rigid anchored joints was on average 32 % greater than the load in flexible ones.

The efficiency of single and bow-tie fan anchors located at the plate end or distributed along the plate into increase strength and ductility of RC slabs was proved by (Smith et al. 2013).

An alternative anchoring solution is represented by the application of a FRP bar placed transversally to the direction of the strengthening in a groove filled with resin according to the Near surface mounted bars technique (Khalifa et al. 1999, 2000). This solution can be reliable when the strengthening-to-concrete width ratio is approaching 1. Different solutions can be performed by positioning the FRP bar on a plane surface or in the corner (see Fig. 6.28). For such a technique a sufficient cover is requested for realizing the groove and installing the NSM bar inside. In (Eshwar et al. 2008) the location of the FRP bar, the grove size and the size of the anchoring bar were investigated in an experimental study. The strength was sensibly increased (also until 50 %) compared with not anchored specimens, even if the best performances were obtained when the anchor bars are located after re-entrant corner (see Fig. 6.28a) instead of before the re-entrant corner (see Fig. 6.28b), larger grooves are executed and more bars applied transversally to the reinforcement. In particular, a minimum groove size varying between 1.5 and 2.5 times the bar anchoring diameter and a minimum of 3 GFRP bars are suggested.

The use of FRP bars as anchoring system could create local concentrated stresses where fibres are turned into the groove with cutting of fibre on the corner

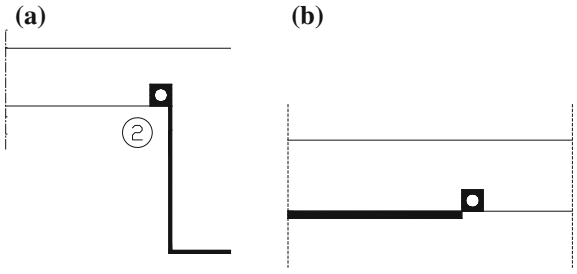

Fig. 6.28 NSM bars for plane surface anchorage for beams/slabs flexural strengthening: **a** after the re-entrant corner; **b** before the re-entrant corner

(Ceroni et al. 2008). However an increasing of ultimate strength at least of 25 % has been experimentally observed if NSM bars are used as end anchorage (Ceroni and Pecce 2010). In Eshwar et al. (2008) a minimum radius of 13 mm is suggested at the corners of the groove to limit stress concentration.

Special Anchorage for Shear Strengthening

For EBR shear strengthening anchoring systems could be particularly useful due to the reduced bond length available in order to avoid debonding. Proper anchorage can be made by systems suitably anchored in the compression zone of the strengthened section.

For shear strengthening solution similar to those proposed for flexural strengthening can be performed. Steel or FRP laminates glued or bolted transversally to the direction of the fibres can be successfully utilized when the not completely wrapped shear reinforcement configuration is adopted.

Special fan anchors can be used also in shear strengthening according to several configurations as tested by Jinno et al. (2001), Kobayshi et al. (2001) to solve the problem of passing fibres of reinforcement through the web of a 'T-section' in order to anchor fibres in the compressive zone (see Fig. 6.29).

Near surface mounted bars have been successfully applied as anchorage systems also at the end of shear strengthening (Fig. 6.30), according to the same applying procedure above described.

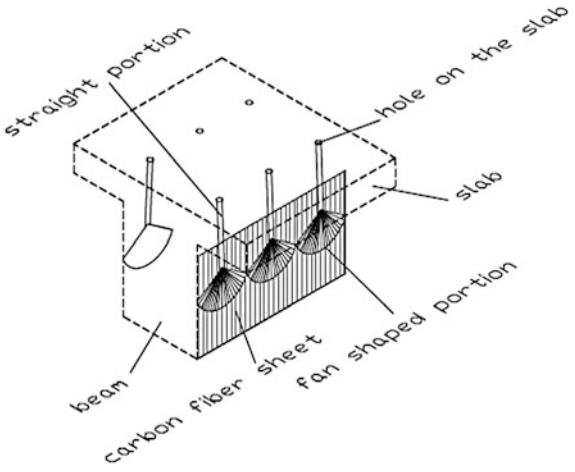

Fig. 6.29 Fan fibres anchors for shear strengthening (Jinno et al. 2001; Kobayshi et al. 2001)

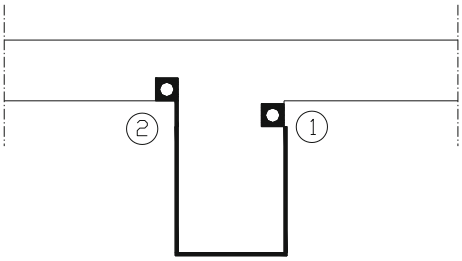

Fig. 6.30 NSM bars as anchors for U-wrap shear strengthening of an R.C. beam

Special Anchorages for Confinement

For confinement of columns where walls physically obstacle the complete wrapping of the elements, application of fan fibres (Jinno et al. 2001; Kobayshi et al. 2001) can give continuity to the reinforcement (see Fig. 6.31a).

Since the application of EBR on rectangular columns or pier walls with large aspect ratio does not actually confine the internal concrete, the EBR jacket need to be constrained on both sides along the length through the use of dowels or bolts or spike anchors. Such systems anchor the jacket to the pre-existing structure, thereby creating shorter distances which are confined between bolts (Fig. 6.31b). The positive effect of fibre anchors on the strength enhancement of wall-like columns confined with FRP was tested by (Tan 2002).

Spike anchors provide a low cost solution also to anchor the confinement jacket to the existing structure and has been tested with very good results for the attachment of FRP jackets at the reentrant corners of L-shaped cross section columns (Karantzikis et al. 2005). Experimental tests evidenced that the partial depth

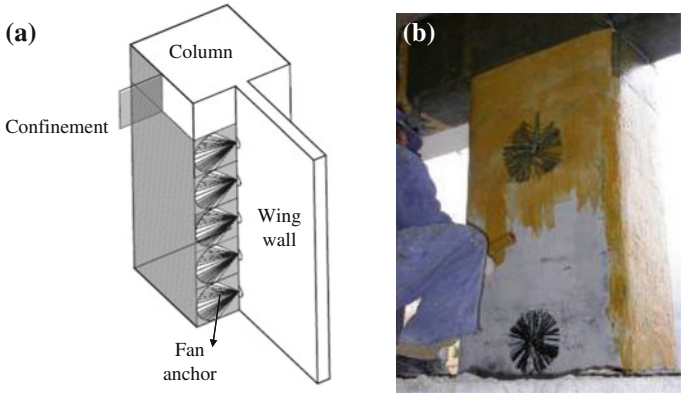

Fig. 6.31 **a** Fibre fan anchor device for confinement of columns; **b** fibre fan splayed on the confining strengthening

anchors give a good effectiveness in terms of deformability and strength increasing, while the benefit provided by full depth anchors are not justified by the high difficulty of installation.

Special Anchorages for Flexural Strengthening of Columns

The anchorage of flexural reinforcement of footing-column/wall joints should be provided. Possible solutions based on the use of steel spike anchors (Fig. 6.32) were tested by (Prota et al. 2005), where the flexural reinforcement was successively wrapped with a FRP jacket, and by (Ascione and Berardi 2011), where the FRP composite was bonded to the device steel plates bolted to each other (double lap bolted joint, see Fig. 6.33).

The flexural strengthening of columns can be realized also with NSM CFRP rods that can be anchored at the beam-column joint by wrapping the end with FRP carbon sheets (Prota et al. 2004).

In Antoniades et al. (2003, 2005) U-shaped devices made by FRP fibres or by steel or FRP laminates glued or bolted were successfully tested as anchoring

Fig. 6.32 Flexural strengthening at the footing joint of a RC column using steel spikes wrapped with a FRP jacket (Prota et al. 2005)

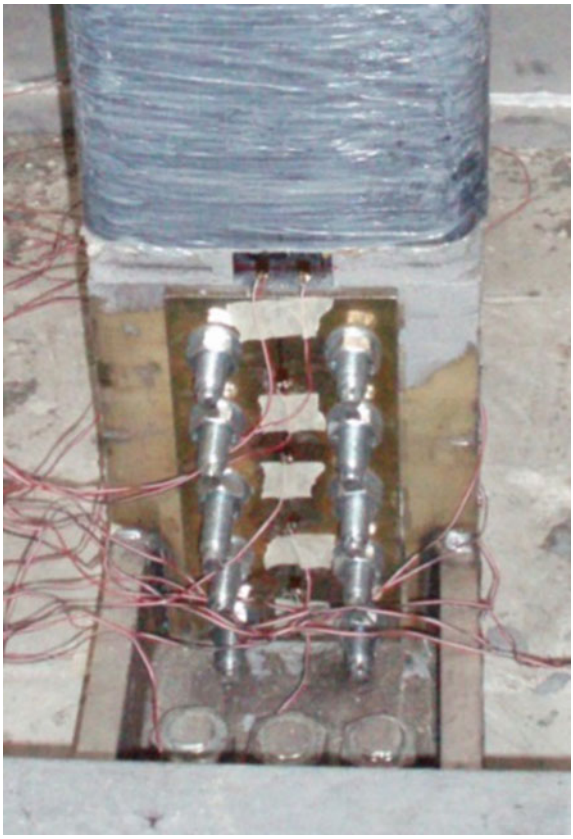

Fig. 6.33 Flexural strengthening of a RC column using anchorage device (Ascione and Berardi 2011)

systems of flexural reinforcement of column and walls at the footing zone. Effectiveness of bolted laminates into improve bond of FRP laminates in flexural strengthening of RC walls was tested by Tan et al. (2003) and Nagy-Gyorgy (2005).

Mechanically Fastened Systems

Description of the MF-FRP System

The implementation of mechanically fastened Fibre Reinforced Polymer (MF-FRP) systems for the flexural strengthening of RC members has emerged as an alternative to FRP materials adhesively bonded to the concrete substrate. The MF-FRP system consists of pre-cured FRP laminates with enhanced bearing strength that are connected to the concrete substrate by means of steel nails, anchor bolts, concrete screws, or combinations thereof.

Compared to the adhesive bonding FRP method, the benefit of MF-FRP is the speed of installation with unskilled labour, minimal or absent surface preparation under any meteorological condition and immediate use of the strengthened structures; also, the MF-FRP system is less vulnerable to fail prematurely by FRP delamination, which abruptly reduces the flexural strength gain and affects the member ductility. Some of the potential shortcomings are: possible concrete damage during anchoring and limited opportunity of installation in the presence of congested internal reinforcement in the members to be strengthened. Laboratory testing and a number of field applications have shown the effectiveness of the MF-FRP method.

FRP Strips

Unidirectional pultruded laminates currently used to be adhesively bonded onto the concrete surface are not suitable to be mechanically attached with steel anchors. These laminates are designed to have high modulus and strength in the longitudinal direction and low mechanical properties in the transverse direction of the laminate. Consequently, unless reinforcing fibres in the transverse direction of the laminate are inserted to provide adequate bearing strength, the orthotropic nature of the material causes the splitting failure of the laminate when a fastener is driven through it (Lamanna 2002). Precured laminates commercially available for strengthening with MF-FRP systems were developed in collaboration with Strongwell (USA, www.strongwell.com) and consist of a glass and carbon hybrid pultruded strip embebbed in a vinyl ester resin (see Fig. 6.34). The one shown has thickness and width of 3.2 and 101.6 mm, respectively; the 3.2 mm width is a suitable size for handling in the field. Continuous glass fibre strand mats are used to provide transverse and bearing strength, while 16–113 yield E-glass roving and 40–48 k standard modulus carbon tows are utilized to provide longitudinal strength and stiffness.

Table 6.10 summarizes the relevant mechanical properties of the FRP strips (Arora 2003). More details about the mechanical characterization of the FRP

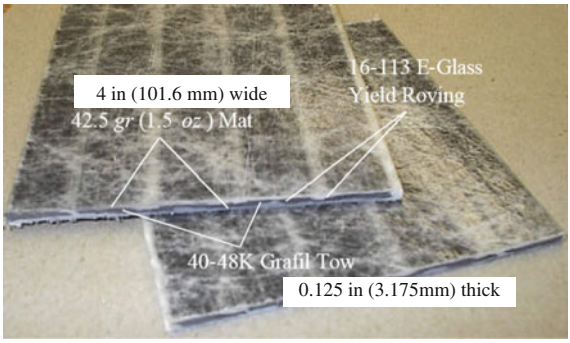

Fig. 6.34 Laminate available for the MF-FRP system

Table 6.10 Properties of FRP strips (Arora 2003)

Ultimate strength		Open-hole strength		Sustained bearing strength		Modulus of elasticity	
Mean (MPa)	COV (%)	Mean (MPa)	COV (%)	Mean (MPa)	COV (%)	Mean (GPa)	COV (%)
844	9.2	640	7.6	234	4.3	61.3	8.6

laminate in the longitudinal and transverse direction can be found in some papers (Arora 2003; Rizzo 2005; Rizzo et al. 2005a).

Fasteners

As mentioned earlier, fastener types that have been investigated for the MF FRP systems include: power-actuated fasteners (PAF), wedge bolts and wedge anchors (see Fig. 6.35).

The PAF system consists of pins embedded into base materials by means of a gunpowder charge. The effects of fastener type, washer, diameter, length, embedment depth have been investigated and discussed elsewhere (Lamanna et al. 2001; Lamanna 2002). Pre-drilling holes in the concrete is strongly recommended in order to reduce detrimental cracking phenomena. The use of the PAF system is particularly suitable when the compression strength of the concrete is less than 27 MPa. The presence of hard aggregates can prevent the fasteners to fully penetrate the concrete substrate (Bank 2004). The PAF installation requires times shorter than for wedge bolts and wedge anchors.

Wedge bolts are single-piece, heavy duty anchors that are driven into pre-drilled holes. Driving of the wedge bolt can be performed with a common rotary drill or impact wrench. As for the PAFs, the efficiency of wedge bolts is dependent on the presence of hard aggregates. Preliminary studies (Rizzo et al. 2005b) indicate that the use is not recommended for concrete with compression strength greater than 27 MPa, and with hard aggregates in the mix design.

In spite of longer installation times, wedge anchors can be used for any type of concrete; they are driven through the laminate into predrilled holes until the nut and

Fig. 6.35 Fasteners used for MF-FRP systems

washer are firmly secured against the laminate. The anchors are typically tightened by turning the nut with an electrical drill with torque control, according to the specifications of fastener manufactures.

Failure Modes of FRP-Fastener-Concrete Connection

The behaviour of MF-FRP connections is related to any of the components constituting the connection, which are the concrete substrate, the fastener and the FRP material. As a result, failure modes can involve the concrete, the yielding/rupture of fastener, or the FRP laminate.

The pry-out or spalling of the concrete (Fig. 6.36a) depends on the local composition of the concrete surface around the fastener. Once pry-out failure develops, the fastener rotates and the FRP laminate pulls it out of the concrete. Several factors promote the initiation of the concrete failure, such as a fastener hitting a hard aggregate during installation, low concrete strength, cracked concrete substrate conditions, short edge distance that may cause spalling, and poor fastener embedment depth (Lamanna 2002; Arora 2003).

The fastener failure usually occurs for deep embedment length, low steel strength and large edge distance (Rizzo 2005).

Four typical failure modes can involve the MF-FRP laminate (Fig. 6.36b): net-tension, cleavage-tension (or block shear), bearing and shear-out. The bearing failure is the most desirable failure mode because the connection is able to maintain its strength until significant levels of displacement (Lamanna 2002; Arora 2003). This failure is characterized by crushing on the material around the bolt-contact area followed by elongation of the hole. The other failure modes tend to develop in a more brittle way (Rosner and Rizkalla 1995). In particular, the net-tension failure is characterized by a fracture in the reduced cross section through the bolt hole, perpendicular to the direction of load. The cleavage failure consists of a crack parallel to the applied load that starts at the edge of the composite and propagates toward the bolt hole, leading to the initiation of other cracks across the net section

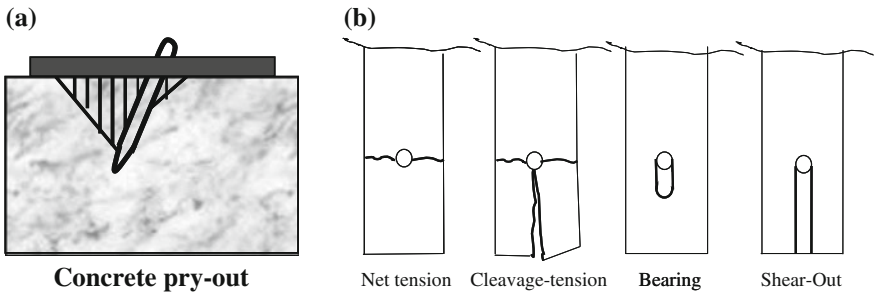

Fig. 6.36 **a** Concrete pry-out failure; **b** typical failure modes of mechanically fastened connections in FRP

due to in-plane stress. This failure mode is attributed to a combination of shear and tensile stress in the material. The shear-out failure, considered as a special case of bearing, is characterized by the formation of two cracks parallel to the applied load that propagate from the bolt hole toward the free edge.

State of Advancement and Current Research

The MF-FRP systems were firstly employed to strengthen RC bridges and infrastructures (Oliva et al. 2003; Rizzo 2005). After the first successful field applications, a number of experimental studies have been performed around the world with the aim of investigating the performance of RC members externally strengthened by MF-FRP laminate and quantifying the benefits obtained in terms of strength, stiffness and displacement capacity (Rizzo 2005; Lamanna et al. 2001, 2004a, b; Martin and Lamanna 2008; Lee et al. 2007).

To this aim, a recently published state-of-the-art review of the experimental research has provided compelling evidence of the effectiveness and viability of using MF-FRP laminates to rehabilitate RC beams and slabs (Brown et al. 2011). In the review, a database of collected test results was assembled to provide a valuable source of information on the performances of MF-FRP strengthened beams and one-way slabs. In a more recent paper, Martinelli et al. (2014) published an updated database of experimental results from four point-bending tests performed on MF-FRP strengthened RC members. As observed, the specimens tested so far have different sizes of the cross-section, with values of the height to-width ratios spanning from 0.5 ("slab" type) to 1.67 ("beam" type"); the clear lengths range from 1067 (small scale members) to 3505 mm (large scale members). The mechanical fastening mostly consists of shot fasteners with diameters ranging from 3.5 to 4.5 mm and lengths from 22 to 47 mm. Screw anchors were also frequently used, for which the diameters span from 4.76 to 12.7 mm and the lengths from 37 to 50.8 mm. Only in a few cases, instead, the mechanically fastening was performed by using wedge anchors (Ekenel et al. 2005; Galati et al. 2007); they were installed into the concrete by using epoxy resin as a gap filler. In these tests, the fasteners were arranged on single or multiple rows (1, 2, 4) according to aligned or staggered configurations or combinations thereof.

From the experimental investigations it has been shown that with appropriate fastener layout and FRP laminate properties, the strength increases are comparable to those of externally bonded-FRP strengthened members but with greater displacements exhibited at collapse. Also, it has been highlighted that the MF-FRP technique allows for preventing the strip delamination before concrete crushing. As an example, the experimental study performed by Napoli et al. (2010) is mentioned (see Fig. 6.37). The authors studied the effects of fastener layout and FRP strip length on flexural strength and deformability and failure mode of MF-FRP strengthened one-way slabs. Concrete screws were used to fasten the FRP strips to the concrete. At failure of specimens, the authors observed that the high

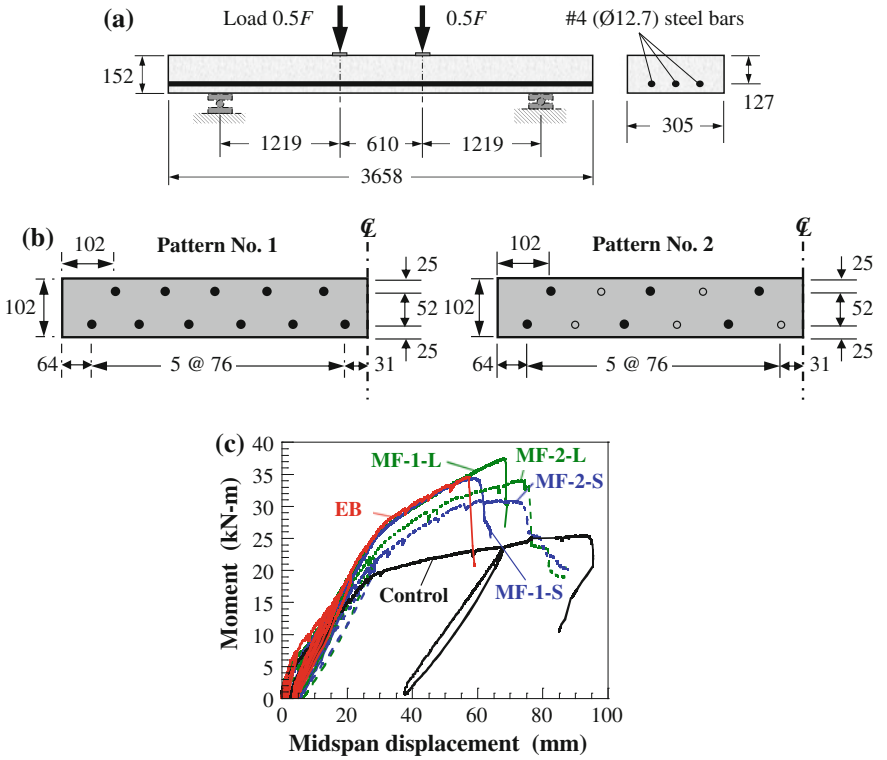

Fig. 6.37 Tests by Napoli et al. (2010): **a** specimens; **b** fastener layouts; **c** results

concentration of shear force caused spalling of the concrete cover but the FRP strip was firmly attached to the member. All MF-FRP strengthened specimens attained ultimate strength levels comparable to that of a benchmark slab strengthened with an externally bonded (EB) carbon FRP laminate, with greater deformability, as shown in Fig. 6.37c. Specimens MF-1L and MF-1S that used a larger number of anchors in the shear span (Pattern No. 1 in Fig. 6.37b), achieved marginally larger ultimate strengths but at lesser deformability than corresponding slabs MF-2L and MF-2S (using Pattern No. 2 in Fig. 6.37b).

Comparative experimental studies (Quattlebaum et al. 2005; Ekenel et al. 2006) on the static and fatigue performance of RC beams strengthened in bending by either MF- or EB-FRP laminates, showed that similar strength levels can be attained.

The feasibility of this strengthening technique was widely demonstrated experimentally in the upgrading of two-way slabs (Elsayed et al. 2009b).

Other experimental investigations examined the suitability of connecting an FRP laminate to the concrete substrate by both adhesive and mechanical anchors (EB + MF-FRP system) (Ekenel et al. 2006; Sena-Cruz et al. 2011; Ebead 2011).

One of the latest studies also showed that the MF-FRP system is viable for strengthening existing reinforced-concrete beams in shear (Johnson 2011).

Also, experimental tests have proven that the mechanically fastened composite system is an effective technique to improve the flexural capacity of corrosion damaged RC beams (El-Maaddawy 2013).

Finally, MF-FRP laminates were recently employed for enhancing the flexural capacity of timber structural members (Dempsey and Scott 2006; Schorer et al. 2008).

Design Rules

Despite the interest and promising experimental results obtained by researchers, there are no international guidelines dealing with MF-FRP till now. However, several analytical and numerical studies have been carried out through years with the aim to predict the flexural behaviour of RC members strengthened with MF-FRP systems: a state-of-the-art review has been recently published in Napoli et al. (2013). As highlighted therein, the first analytical models were based, for the sake of simplicity, on the hypothesis of "conservation of plane sections" between the concrete and the FRP, as generally accepted for EB-FRP strengthened members (Lamanna 2002; Bank et al. 2002; Bank 2004; Bank and Arora 2007; Rizzo et al. 2005b). Despite their ease of application, such models have often provided inaccurate predictions which were primarily attributed to ignoring the slip between the concrete and FRP strip. Therefore, novel proposals accounting for the concrete-FRP interfacial behaviour were recently formulated by (Lee et al. 2009; Nardone et al. 2011).

Lee et al. (2009), after observing and verifying the slip effect at the connection between FRP and concrete, introduced a FRP strain reduction factor calibrated on the basis of experimental results in order to evaluate the nominal moment capacity. However, even after this, an assumed reduction factor can lead to an incorrect evaluation of the neutral axis depth at ultimate limit state and does not provide useful information under service conditions.

Nardone et al. (2011) proposed analytical procedures for the evaluation of the flexural behaviour at both serviceability and ultimate limit states. Their analytical models account for equilibrium, compatibility and constitutive relationships of materials; in particular, they account explicitly for the slip behaviour between the concrete surface and the FRP strip due to the fasteners. The proposed models, coupled with an appropriate computation algorithm, are able to predict the fundamentals of flexural behaviour of RC members strengthened with MF-FRP strips also in terms of load versus deflection curves, failure modes, strain profiles and curvatures.

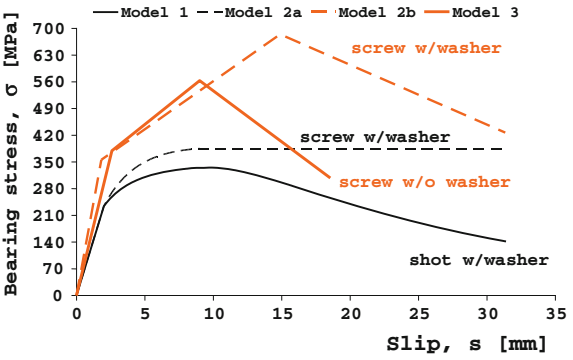

Fig. 6.38 Bearing stress-slip models

The models are capable of predicting the three failure modes experimentally found for well-designed applications, namely: bearing failure or net tension failure of the FRP laminate and concrete crushing.

The comparison between the analytical predictions and the experimental results shows a good agreement in terms of strain profiles in MF-FRP strips and moment deflection curves at serviceability limit state. Similarly, comparison of nominal flexural capacity, ultimate curvature and FRP strain at ultimate limit state show good agreement. This agreement is higher if bearing failure of many fasteners is accepted and included in the evaluations (Nardone et al. 2012). However from a design point of view, it is suggested to design for the desired sustained bearing failure of the first outermost fastener.

The knowledge of the relationship between the force acting on the fastener and the slip is fundamental in order to apply the proposed model and more research to address this fundamental parameter is needed.

To this aim, Elsayed et al. (2009a) and Realfonzo et al. (2013) recently proposed nonlinear bearing stress-slip σ-s models to describe the effect of the partial interaction between the concrete and the FRP laminate. These models, shown in Fig. 6.38, were calibrated by best-fitting experimental results of direct shear tests (DSTs) performed on MF-FRP/concrete joints with a single connector.

Two different σ-s models were found by Elsayed et al. (2009a), suitable for shot (*Model 1*) and screwed (*Model 2a*) fasteners, respectively, both with steel washers (Fig. 6.38). The first model was calibrated for MF-FRP/concrete joints having a single shot fastener with a 47 mm shank length, a 3.7 mm shank diameter and a 13 mm washer where the fastener was driven into the concrete using a powder actuated gun. The second model was for the case of a single screwed fastener with a 37 mm shank length, a 4.8 mm shank diameter and a 16 mm washer installed into the concrete using a drilling tool.

Trilinear σ-s models were proposed by (Realfonzo et al. 2013) for a single screwed fastener with (w/washer) or without (w/o washer) washer (*Models 2b* and *3*

in Fig. 6.38); the screw had a 45 mm shank length, a 6 mm shank diameter, a 32 mm washer (when used) and was driven into the pre-drilled hole using a common torque wrench.

Once the first studies on the FRP-concrete interfacial behaviour were published in the literature, refined moment-deflections models were developed. Among them, the numerical model developed by Napoli et al. (2010) was based on a general algorithm formulated by implementing the differential equation of Newmark's theory for steel-concrete composite beams with linear-elastic shear connectors (Newmark et al. 1951) into an 'exact' two-node finite element (FE) developed for the analysis of partial interaction in composite beams with flexible shear connectors (Faella et al. 2008). The finite element introduced is used for nonlinear analysis through fibre discretization of the beam cross-section, and by implementing an iterative convergence procedure based on the secant value approach to account for material non-linearity, including concrete, steel and concrete-FRP interface. For the latter, the interface bearing stress-slip *Model 2a* in Fig. 6.38 and its resulting simplification in a bilinear law (Napoli et al. 2010) were successfully implemented and verified to evaluate applicability for analysis and design purposes.

A different 1-D numerical model was presented by Martinelli et al. (2014) to explicitly account for the discrete connection between FRP laminate and RC beam. Later, the model was also used by the authors to investigate the cracking process in RC members (and its implications on the structural response including the tension-stiffening effect) which is generally neglected (Martinelli et al. 2013).

Figure 6.39a depicts the considered finite element which is obtained by assembling the following three components: (a) a 1-D element that models the behaviour of an Euler-Bernoulli RC beam; (b) a rod element that simulates the mechanical behaviour of an FRP laminate; (c) two springs used as axial constraints between the FRP laminate and the RC beam. The two springs simulate the behaviour of the fasteners connecting the FRP laminate to points on the beam surface, i.e., at the points where the fasteners are actually screwed or shot. Four degrees of freedom are considered in each node to take into account the possible axial displacements of both RC beams and FRP strips, along with deflections and rotations of the former component. The stiffness matrix of the proposed FE is derived by assembling the key mechanical components of the RC beam/slab, the FRP strip and the mechanical fasteners. The nonlinear behaviour of the aforementioned components and materials is handled through well-established numerical techniques usually adopted in nonlinear FE analysis.

The procedure was validated by comparing the numerical simulations in terms of load-deflection curves with the results of some experimental tests reported in the literature. In particular, Fig. 6.39b shows a comparison for an MF-FRP strengthened slab tested by Napoli et al. (2010). In this case, the behaviour of the screws w/o washers was modelled by adopting the trilinear *Model 3* (Fig. 6.38). For comparison, the nonlinear *Model 1* for shot fasteners (Fig. 6.38) was also considered. It is shown that the numerical simulations do not significantly change with the use of the two different bearing stress-slip relationships, thus suggesting that both of them are suitable to model MF-FRP strengthened members.

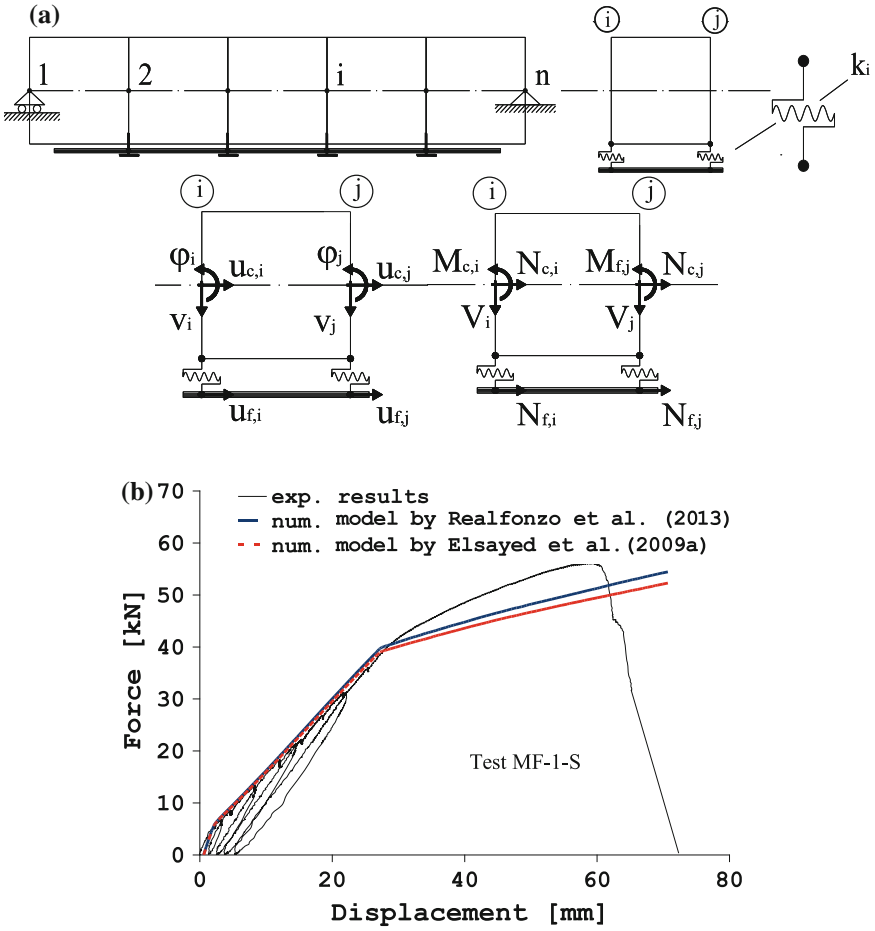

Fig. 6.39 FE model by Martinelli et al. (2014): **a** schematic and **b** validation

References

Serviceability Limit States

ACI (2005). Building code requirements for structural concrete and commentary, ACI 318R-05, ACI Committee 318, Farmington Hills, Mich.

Aiello, M. A., & Ombres, L. (2000). Load deflection analysis of FRP reinforced concrete flexural members. *ASCE Journal of Composite in Construction, 4*(4), 164–171.

Aiello, M. A., & Ombres, L. (2004). Cracking and deformability analysis of reinforced concrete beams strengthened with externally bonded carbon fiber reinforced polymer sheets. *Journal of Materials in Civil Engineering, 16*(5), 392–399.

Balsamo, A., Nardone, F., Iovinella, I., Ceroni, F., & Pecce, M. (2013a). Flexural strengthening of concrete beams with EB-FRP, SRP and SRCM. *Experimental investigation, Composites: Part B* doi:10.1016/j.compositesb.2012.10.014.

Balsamo, A., Bilotta, A., Ceroni, F., Nigro, E., & Pecce M., (2013b). Efficiency of CFRP NSM strips and EBR laminates for flexural strengthening of RC beams. In B. Joaquim & S.-C. José (Eds.), *Proceedings of FRPRCS11*, UM, Guimarães.

Barros, J. A. O., & Fortes, A. S. (2005). Flexural strengthening of concrete beams with CFRP laminates bonded into slits. *Journal Cement and Concrete Composites, 27*(4), 471–480.

Barros, J. A. O., Dias, S. J. E., & Lima, J. L. T. (2007). Efficacy of CFRP-based techniques for the flexural and shear strengthening of concrete beams. *Journal Cement and Concrete Composites, 29*(3), 203–217.

Bischoff, P. H. (2007). Deflection calculation of FRP reinforced concrete beams based on modifications to the existing Branson equation. *ASCE Journal of Composites for Constructions, 11*(1), 4–14.

Borchert, K. (2007). Bond behaviour of adhesively bonded reinforcement in service. Ph.D. Thesis, Technische Universität München (in German with English summary).

Borchert, K., & Zilch, K. (2008). Bond behaviour of NSM FRP strips in service. *Structural Concrete, 9*, 128–142.

Branson, D. E. (1977). *Deformations of concrete structures* (pp. 167–169). New York: McGraw-Hill.

Charkas, H., Rasheed, H. A., & Melhem, H. (2003). Rigorous procedure for calculating deflections of fiber-reinforced polymer-strengthened reinforced concrete beams. *ACI Structural Journal, 100*(4), 529–539.

fib bulletin No. 65. (2012). Model Code 2010-Final draft, Volume 1, International Federation for Structural Concrete, Lausanne, Switzerland. ISSN 1562-3610. ISBN:978-2-88394-105-2.

fib bulletin No. 66. (2012). Model Code 2010-Final draft, Volume 2, International Federation for Structural Concrete, Lausanne, Switzerland. ISSN 1562-3610. ISBN:978-2-88394-105-2.

Ceroni, F., Pecce, M., & Matthys, S. (2004). Tension stiffening of RC ties strengthened with externally bonded FRP sheets. *ASCE Journal of Composites for Constructions, 8*(1), 22–32.

Ceroni, F., & Pecce, M. (2004). Modelling of tension stiffening behaviour of RC ties strengthened with FRP sheets. *ASCE Journal of Composites for Constructions, 8*(6), 510–518.

Ceroni, F., & Pecce, M. (2007). Cracking behaviour of RC beams externally strengthened with emerging materials. *Construction and Building Materials, 21*(4), 736–745.

Ceroni, F., & Pecce, M. (2009). Design provisions for crack spacing and width in RC elements externally bonded with FRP. *Composites Part B, 40*(1), 17–28.

Ceroni, F. (2010). Experimental performances of RC beams strengthened with FRP materials. *Construction and Building Material, 24*, 1547–1559.

CNR DT 200/R1. (2012). Guide for the Design and Construction of Externally Bonded FRP Systems for Strengthening Existing Structures, Advisory Committee on Technical Recommendation for Construction of National Research council, Rome, Italy.

Eligehausen, R., Popov, E. P., & Bertero, V. V. (1983). Local bond stress-slip relationships of deformed bars under generalized excitations, Report no. 83/23, EERC. University of California, Berkeley.

El-Mihilmy, M. T., & Tedesco, J. W. (2000). Deflection of reinforced concrete beams strengthened with fiber-reinforced polymer (FRP) plates. *ACI Structural Journal*, *97*(5).

EN 1990. (2002). Eurocode 0: Basis of Structural Design, European Committee of Standardization.

Ferretti, D., & Savoia, M. (2003). Cracking evolution in R/C tensile members strengthened by FRP-plates. *Engineering Fracture Mechanics, 70*, 1069–1083.

Ferrier, E., Avril, S., Hamelin, P., & Vautrin, A. (2003). Mechanical behavior of rc beams reinforced by externally bonded CFRP sheets. *Materials and Structures/Matériaux and Constructions, 36*(262), 522–529.

Jourawski, D. J. (1858). Sur le résistance d'un corps prismatique et d'une Piece Composée en Bois ou on Tôle de Fer à une Force Perpendiculaire à leur Longeur, Annales des Ponts et Chausees, Memoires and Documents, 3rd Series, V. 12, Part 2, pp. 328–351

Kim, Y. J., Shi, C., & Green, M. F. (2008a). Ductility and cracking behavior of prestressed concrete beams strengthened with prestressed CFRP sheets. *ASCE Journal of Composites for Construction, 12*(3), 274–283.

Matthys, S. (2000). Structural behaviour and design of concrete members strengthened with externally bonded FRP reinforcement, Ph Doctoral thesis, Faculty of Engineering, Department of Structural Engineering, Ghent University, Ghent, Belgium.

Monti, G., Alessandri, S., & Santini, S. (2009). Design by testing: a procedure for the statistical determination of capacity models. *Construction and Building Materials, 23*(4), 1487–1494.

Pecce, M., Ceroni, F., Prota, A., & Manfredi, G. (2006). Response prediction of RC beams externally bonded with steel reinforced polymers. *ASCE Journal of Composites for Construction, 10*(3), 195–203.

Rasheed, A. H., Charkas, H., & Melhem, H. (2004). Simplified nonlinear analysis of strengthened concrete beams based on a rigorous approach. *ASCE Journal of Structural Engineering, 130* (7), 1087–1096.

Razaqpur, A. G., Švecová, D., & Cheung, M. S. (2000). Rational method for calculating deflection of fiber-reinforced polymer reinforced beams. *ACI Structural Journal, 97*(1), 175–184.

Roberts, T. M. (1989). Approximate analysis of shear and normal stress concentrations in the adhesive layer of plated RC beams. *The Structural Engineer, 67*(12), 229–233.

Sato, Y., Ueda, T., & Shoji, K. (2002). Tension stiffening effect of reinforced concrete member strengthened by carbon fiber sheet. In *Proceedings of the International Symposium "Bond in concrete", Budapest*, 20–22 November 2002, pp. 606–613.

Täljsten, B. (2004). FRP Strengthening of existing concrete structures: design guideline. Lulea University of Technology. ISSN 91-89580-03-4.

Tan, K. H., & Saha, M. K. (2008). Cracking characteristics of RC beams strengthened with FRP system. *Journal of Composites for Construction, 12*(5), 513–521.

Tripi, J. M., Bakis, C. E., Boothby, T. E., & Nanni, A. (2000). Deformation in concrete with external CFRP sheet reinforcement. *ASCE Journal of Composites for Construction, 4*(2), 85–94.

Ueda, T., Yamaguchi, R., Shoji, K., & Sato, Y. (2002). Study on behavior in tension of reinforced concrete members strengthened by carbon fiber sheet. *ASCE Journal of Composites for Construction*, *6*(3), 168–174.

Yoshizawa, H., & Wu, Z. (1999). Crack behavior of plain concrete and reinforced concrete members strengthened with carbon fiber sheets. *Proceedings of Fourth International Symposium on FRP Reinforcement*, Vol. 1, pp. 767–779

Zehetmaier, G., & Zilch, K. (2008). Rissbildung und Rissbreitenbeschränkung bei Verstärkung mit CFK-Lamellen. *Bauingenieur, 83*, 19–26.

Zhang, Y., Toutanji, H., & Balagrou, P. (2003). Crack widths in R.C. beams externally bonded with CFRP sheets. *Proceedings of FRPRCS-6*, Singapore, 8–10 July 2003.

Fatigue Behaviour

ACI Committee 440. (2008). Guide for the Design and Construction of Externally Bonded FRP Systems for Strengthening Concrete Structures.

Ali-Ahmad M., et al. (2006), Experimental investigation and fracture analysis of debonding between concrete and FRP. *Journal of Engineering Mechanics ASCE*, *132*(9), 914–923.

Anderson, T. L. (2004). *Fracture mechanics: fundamentals and applications*. Boca Raton: CRC Press.

Bizindavyi, L., et al. (2003), Experimental investigation of bonded fiber reinforced polymer-concrete joints under cyclic. *Journal of Composites in Construction*, pp. 127–133.

Budelmann, H., et al. (2013). *Praxisgerechte Bemessungsansätze für das wirtschaftliche Verstärken von Betonbauteilen mit geklebter Bewehrung - Verbundtragfähigkeit unter dynamischer Belastung, DAfStb Heft 593*. Berlin: Beuth Verlag.

Carloni, C., et al. (2012). Experimental determination of FRP concrete cohesive interface properties under fatigue loading. *Composite Structures, 94*(4), 1288–1296.

Carloni C., et al.. (2013). Sub-critical fatigue crack growth in FRP/concrete cohesive interface. *Composite: Part B*, *51*, 35–43.

CNR-DT 200. (2004). Guide for the design and construction of externally bonded FRP systems for strengthening existing structures.

Dai, J. G., et al. (2005). Static and fatigue bond characteristics of interfaces between CFRP sheets and frost damage experienced concrete. *Proceedings of 7th International Symposium on Fiber Reinforced Polymer Reinforcement for Reinforced Concrete Structures, Kansas City*, MO, American Concrete Institute (ACI), Farmington Hills, MI, 15151530.

Diab, H. M., et al. (2009). Theoretical solution for fatigue debonding growth and fatigue life prediction of FRP-concrete interfaces. *Advanced Structural Engineering*, *12*(6), 781–792.

Ferrier, E., et al. (2005). Fatigue of CFRPs externally bonded to concrete. *Materials and Structures, 38*, 39–46.

fib Task Group 9.3 FRP, bulletin 14. (2001). Externally bonded FRP reinforcement for RC structures.

DAfStb-guideline. (2012). *DAfStb Guideline On the Strengthening of Concrete Members with Adhesively Bonded Reinforcement*. German Committee for Structural Concrete, Berlin: Beuth Verlag.

German Committee for Structural Concrete. (2013). *Commentary on the DAfStb Guideline Strengthening of Concrete Members with Adhesively Bonded Reinforcement with Examples, Report 595*. Berlin: Beuth Verlag.

Hankers, C. (1996). Zum Verbundtragverhalten laschenverstärkter Betonbauteile unter nicht vorwiegend ruhender Beanspruchung, Dissertation, Institut für Baustoffe, Massivbau und Brandschutz, TU Braunschweig.

Heffernan, P. J., et al. (2004). Fatigue behavior of reinforced concrete beams strengthened with carbon fiber reinforced plastic laminates. *Journal of Composites in Construction, 8*, 132–140.

Kim, Y. J., Heffernan, P. J. (2008). Fatigue behavior of externally strengthened concrete beams with fiber-reinforced polymers: state of the art. *Journal of Composites in Construction, 12*, 246–256.

ISIS Canada. (2001), Strengthening reinforced concrete structures with externally-bonded fibre reinforced polymers: Design manual No. 4.

Ko, H. (2007). Bond stress slip relationship between frp sheet and concrete under cyclic load. *Journal of Composites for Construction*, *11*(4), 419–426.

Sutton, M. A. et al. (1983). Determination of displacements using an improved digital correlation method. *Image Vision Computing*, *1*(3), 133–139.

Sutton, M. A., et al. (2009). *Image correlation for shape, motion and deformation measurements*. New York: Springer.

Wu, Z., et al. (2010). Tensile fatigue behavior of FRP and hybrid FRP sheets. *Composites: Part B, 41*, 396402.

Yao, J., et al. (2005). Experimental study on FRP-to-concrete bonded joints. *Composites Part B Engineering, 36*(2), 99–113.

Effects of Fire and High Temperature

ACI 318-11. (2013). Building Code Requirements for Structural Concrete and Commentary, ISBN-13 978-0870317446.

Bai, Y., Vallée, T., & Keller, T. (2007). Modeling of thermo-physical properties for FRP composites under elevated and high temperature. *Composites Science and Technology, 67*, 3098–3109.

Bisby, L. A., Green, M. F., Kodur, V. K. R. (2005). Response to fire of concrete structures that incorporate FRP. *Progress in Structural Engineering and Materials*, *7*(3), 136–149.

Blontrock, H., Taerwe, L., & Vandevelde, P. (2001). Fire testing of concrete slabs strengthened with fibre composite laminates. *Proceedings of 5th International Conference on Fibre Reinforced Plastics for Reinforced Concrete Structures,* Telford, Cambridge, U.K., pp. 547–556.

Cleary, D. B., Cassino, C. D., & Tortorice, R. (2003). Effect of elevated temperature on a fiber composite used to strengthen concrete columns. *Journal of Reinforced Plastics and Composites, 2210*, 881–895.

Dai, J. G., Sato, Y., Ueda, T., & Sato, Y. (2005). Static and fatigue bond characteristics of interfaces between CFRP sheets and frost damage experienced concrete. *Proceedings of FRPRCS-7, ACI-SP-230-86*, pp. 1515–1530.

Dai, J. G., Gao, W. Y., Teng, J. G. (2013). Bond-slip model for FRP laminates externally bonded to concrete at elevated temperature. *Journal of Composites for Construction, 17*(2). © ASCE, ISSN 1090-0268/2013/2-217-228.

Deuring, M. (1993). Brandversuche an nachtraglich verstarkten tragern aus beton. Research Rep. No. 148'795, EMPA, Dubendorf, Switzerland.

EN 1992-1-2. Eurocode 2. Design of concrete structures – Part 1-2: General Rules – Structural Fire Design, European committee for standardization, March, 2004.

Gamage, J. C. P. H., Wong, M. B., & Al-Mahaidi, R. (2005). Performance of CFRP strengthened concrete members under elevated temperatures. *Proceedings of International Symposium on Bond Behaviour of FRP in Structures*, IIFC, Hong Kong, pp. 113–118.

Jia, J., Boothby, T. E., Bakis, C. E., & Brown T. L. (2005). Durability evaluation of glass fiber reinforced-polymer-concrete bonded interfaces. *Journal of Composites for Construction*, *9*(4). ©ASCE, ISSN 1090-0268/2005/4-348–359.

Kodur, V. K. R., Bisby, L. A., & Green, M. F. (2007). Guidance for the design of FRP-strengthened concrete members exposed to fire. *Journal of Fire Protection Engineering, 175*, 5–26.

Mouritz, A. P., & Gibson, A. G. (2006). *Fire properties of polymer composite materials*. New York: Springer.

Mouritz, A. P., & Mathys, Z. (1999). Postfire mechanical properties of marine polymer composites. *Composite Structures, 471*, 643–653.

NTC. (2008). D.M.14/1/2008 "Norme Tecniche per le Costruzioni" (Testo integrato con la Circolare n°617/C.S.LL.PP. del 2/2/2009).

Nigro, E., Cefarelli, G., Bilotta, A., Manfredi, G., & Cosenza, E. (2011a). Fire resistance of concrete slabs reinforced with FRP bars. Part I: experimental investigations on the mechanical behaviour. *Composites: Part B*, *Engineering*, *42*, 1739–1750. doi:10.1016/j.compositesb.2011.02.025. ISSN 1359-8368.

Nigro, E., Cefarelli, G., Bilotta, A., Manfredi, G., & Cosenza, E. (2011b). Fire resistance of concrete slabs reinforced with FRP bars. Part II: experimental results and numerical simulations on the thermal field. *Composites: Part B*, *Engineering*, *42*, 1751–1763. doi:10.1016/j.compositesb.2011.02.026. ISSN 1359-8368.

Nigro, E., Cefarelli, G., Bilotta, A., Manfredi, G., & Cosenza, E. (2013). Adhesion at high temperature of FRP bars straight or bent at the end of concrete slabs. *Journal of Structural Fire Engineering*, pp. 71–86. doi:10.1260/2040-2317.4.2.71. ISSN 2040-2317.

Nigro, E., Bilotta, A., & Del Prete, I. (2013a). Flexural check at high temperatures of reinforced concrete bridge decks strengthened with EBR-FRP. Applications of Structural Fire Engineering, 19–20 April 2013, Prague, Czech Republic.

Nigro, E., Bilotta, A., & Del Prete, I. (2013b). High temperature effects on flexural performances of RC bridge decks strengthened with EBR-FRP. ACI Italy Chapter. Bergamo 3-4 October 2013.

Porter, M. L., & Harries, K. A. (2005). *Workshop on research in FRP composites in concrete construction*. Arlington: National Science Foundation.

Saafi, M., & Romine, P. (2002). Effect of fire on concrete cylinders confined with GFRP. *Proceedings of 2nd International Conference on Durability of Fibre Reinforced Polymer (FRP) Composites for Construction*, Université de Sherbrooke, pp. 512–521.

Long Term Properties of FRP Systems

ASTM D 638. (2003). Standard Test Methods for Tensile Properties of Plastics. *American Society for Testing and Materials* (ASTM), Pennsylvania, US.

ASTM 2990. (2001). Standard Test Methods for Tensile, Compressive, and Flexural Creep and Creep-Rupture of Plastics. *American Society for Testing and Materials* (ASTM), Pennsylvania, US, 20 pp.

Brinson, H. F., & Brinson, L. C. (2008). *Polymer engineering science and viscoelasticity: an introduction*. New York: Springer Science + Business Media.

Choi, K.-K., Meshgin, P., & Taha, M. M. R. (2007). Shear creep of epoxy as the concrete-FRP interfaces. *Composites Part B: Engineering, 38*(5–6), 772–780.

Costa, I. G. (2014). Prestressed carbon fibre laminates applied according to near surface mounted technique to increase the flexural resistance of reinforced concrete beams. Ph.D. Thesis, University of Minho.

Costa, I. G., & Barros, J. A. O. (2013). Assessment of the long term behaviour of structural adhesives in the context of NSM flexural strengthening technique with prestressed CFRP laminates. FRPRCS11, Guimarães, Portugal.

Costa, I. G., & Barros, J. A. O. (2011). Creep of Adhesives: Review. *Report 11-DEC/E-03*, University of Minho, Guimarães, Portugal, 39 pp.

Diab, H., & Wu, Z. (2007). A linear viscoelastic model for interfacial long-term behavior of FRP–concrete interface. *Composites Part B: Engineering, 39*(4), 722–730.

Dolan, C. W., Hamilton, H. R., Bakis, C. E., & Nanni, A. (2001). Design recommendations for concrete structures prestressed with FRP tendons. *FHWA-DTFH61-96-C-00019*, Federal Highway Administration, Washington, DC.

Feng, C. W., Keong, C. W., Hsueh, Y. P., Wang, Y. Y., & Sue, H. J. (2005). Modeling of long-term creep behavior of structural epoxy adhesives. *International Journal of Adhesion and Adhesives, 25*(5), 427–436.

ISO 527-2. (1993). Plastics: Determination of tensile properties—Part 2: Test conditions for moulding and extrusion plastics. *International Organization for Standardization* (ISO), Geneva, SZ, 8 pp.

ISO 899-1. (2003). Plastics: Determination of creep behaviour—Part 1: Tensile creep. *International Organization for Standardization* (ISO), Geneva, SZ.

Khoun, L., & Hubert, P. (2010). Cure shrinkage characterization of an epoxy resin system by two in situ measurement methods. *Polymer Composites*, *31*(9), 1603–1610.

Li, C., Potter, K., Wisnom, M. R., & Stringer, G. (2004). In-situ measurement of chemical shrinkage of MY750 epoxy resin by a novel gravimetric method. *Composites Science and Technology, 64*(1), 55–64.

Lopez-Anido, R. A., & Naik, T. R. (2000). *Emerging Materials for Civil Engineering Infrastructure: State of the Art*. Reston: American Society of Civil Engineers.

Majda, P., & Skrodzewicz, J. (2009). A modified creep model of epoxy adhesive at ambient temperature. *International Journal of Adhesion and Adhesives, 29*(4), 396–404.

Meaud, C., Jurkiewiez, B., & Ferrier, E. (2011). Investigation of creep effects in strengthened RC structures through double lap shear testing. *Composites Part B: Engineering, 42*(3), 359–366.

Sayed-Ahmed, E. Y. (2002). Single and Multi-Strand Steel Anchorage Systems for CFRP Tendons/Stays. *4th Structural Speciality Conference of the Canadian Society for Civil Engineering*, Montréal, Québec, 5–8 June, 10 pp.

Wang, W.-W., Dai, J.-G., Harries, K. A., & Bao, Q.-H. (2012). Prestress losses and flexural behavior of reinforced concrete beams strengthened with posttensioned CFRP sheets. *Journal of Composites for Construction, ASCE, 16*(2), 207–216.

Wu, Z., & Diab, H. (2007). A linear viscoelastic model for interfacial long-term behavior of FRP-concrete interface. *Journal of Composites for Construction, ASCE, 11*(5), 477–486.

Yu, H., Mhaisalkar, S., & Wong, E. (2005). Cure shrinkage measurement of nonconductive adhesives by means of a thermomechanical analyzer. *Journal of Electronic Materials, 38*(4), 1177–1182.

Anchorage Systems for External Strengthening with FRP

Ascione, L., & Berardi, V. P. (2011). Anchorage device for FRP laminates in the strengthening of concrete structures close to beam-column joints. *Composites Part B: Engineering*, *42*(7), 1840–1850.

Al-Mahaidi, R., & Kalfat, R. (2011). Investigation into CFRP plate end anchorage utilizing uni-directional fabric wrap. *Composite Structures, 93*(2), 821–830.

Antoniades, K. K., Salonikios, T. N., & Kappos, A. J. (2003). Cyclic tests on seismically damaged R/C walls strengthened using fiber reinforced polymer reinforcement. *ACI Structural Journal, 100*(4), 510–518.

Antoniades, K. K., Salonikios, T. N., & Kappos, A. J. (2005). Tests on seismically damaged reinforced concrete walls repaired and strengthened using fiber-reinforced polymers. *Journal of Composites for Construction, 9*(3), 236–246.

Bank, L. C. (2004). Mechanically-fastened FRP (MF-FRP): a viable alternative for strengthening RC members. In Seracino (Ed.), *Proceedings of the International Conference FRP Composites in Civil engineering, CICE 2004, Adelaide*, Australia, 8–10 December 2004, pp. 3–15. Taylor & Francis Group, London. ISBN 90 5809 638 6.

Blaschko. M. (2001). Anchorage device for FRP strips. In T. Telford (Ed.), *Proceedings of the Fifth Conference on Non-Metallic Reinforcement for Concrete Structures*, *Proceedings of FRPRCS5 International symposium*, Cambridge, UK, Vol. 2, pp. 1255–1264.

Bonaldo, E., Barros, J. A. O., & Lourenço, P. J. B. (2008). Efficient strengthening technique to increase the flexural resistance of existing RC slabs. *Journal of Composites for Construction, 12*(2), 149–159.

Ceroni, F. (2010). Experimental performances of RC beams strengthened with FRP materials. *Construction and Building Material, 24*, 1547–1559.

Ceroni, F., Pecce, M., Matthys, S., & Taerwe, L. (2008). Bond tests on concrete elements with CFRP and anchorage systems. *Composites: Part B, 39*, 429–441.

Ceroni, F., & Pecce, M. (2010). Evaluation of bond strength and anchorage systems in concrete elements strengthened with CFRP sheets. *Journal of Composites in Construction, ASCE, 14*(5), 521–530.

Eshwar, N., Nanni, A., & Ibell, T. J. (2008). Performance of two anchor systems of externally bonded fiber-reinforced polymer laminates. *ACI Materials Journal.*

Jinno, Y., Tsukagoshi, H., & Yabe, Y. (2001). RC beams with slabs strengthened by CF sheets and bundles of CF strands. In T. Telford (Ed.), *Proceedings of FRPRCS-5 International symposium,* July 2001, Cambridge, UK, pp. 981–987.

Karantzikis, M., Papanicolaou, C. G., Antonopoulos, C. P., & Triantafillou, T. C. (2005). Experimental investigation of nonconventional confinement for concrete using FRP. *ASCE Journal of Composite for Construction*.

Khalifa, A., Belarbi, A., & Nanni, A. (2000). Shear performance of RC members strengthened with externally bonded FRP wraps. *Proceedings of 12WCEE Conference*.

Khalifa, A., Alkhrdaji, A., Nanni, A., & Lansburg, S. (1999). Anchorage of surface mounted FRP reinforcement. *Concrete International: Design and Construction, 21*(10), 49–54.

Kim, Y. J., Wight, R. G., & Green, M. F. (2008). Flexural strengthening of RC beams with prestressed CFRP sheets: using nonmetallic anchor systems. *ASCE Journal of Composites for Construction, 12*(1), 44–52.

Kobayshi, K., Fujii, S., Yabe, Y., Tukagoshi, H., & Sugiyama, T. (2001). Advanced wrapping system with CF-anchor: stress transfer mechanism of CF-anchor. In T. Telford (Ed.), *Proceedings of FRPRCS5 International symposium,* July 2001, Cambridge, UK.

Mukhopadhyaya, P., Swamy, N., & Lynsdale, C. (1998). Optimizing structural response of beams strengthened with GFRP plates. *Journal of composites for construction*.

Nagy-Gyorgy, T., Mosoarca, M., Stoian, V., Gergely, J., & Dan, D. (2005). Retrofit of reinforced concrete shear walls with CFRP composites. *Proceedings of fib Symposium "Keep concrete Attractive,* Budapest, Hungary, 23–25 May 2005, pp. 897–902.

Niemitz, C. W., James, R., & Breña, S. F. (2010). Experimental behavior of carbon fiber-reinforced polymer CFRP sheets attached to concrete surfaces using CFRP anchors. *Journal of Composites for Construction, 14*(2), 185–194.

Orton, S. L., Jirsa, J. O., & Bayrak, O. (2008). Design considerations of carbon fiber anchors. *ASCE Journal of Composites for Construction, 12*(6), 608–616.

Özdemir, G. (2005). Mechanical Properties of CFRP Anchorages, Master of Science Thesis, Middle East Technical University, Istanbul Turkey.

Prota, A., Nanni, A., Manfredi, G., & Cosenza, E. (2004). Selective upgrade of undersigned reinforced concrete beam-column joints using carbon fiber reinforced polymers. *ACI Structural Journal, 101*(5), 699–707.

Prota, A., Tan, K., Nanni, A., Pecce, M., & Manfredi, G. (2006). Performance of RC shallow beams externally bonded with steel reinforced polymer. ACI Structural Journal.

Prota, A., Manfredi, G., Balsamo, A., Nanni, A., & Cosenza, E. (2005). Innovative technique for seismic upgrade of RC square columns. *Proceedings of FRPRCS7*.

Smith, S., Zhang, H., & Wang, Z. (2013). Influence of FRP anchors on the strength and ductility of FRP-strengthened RC slabs. *Construction and Building Materials, 49*, 998–1012.

Tan, K. H. (2001). Details of FRP reinforcement: an overview. In J. G. Teng (Ed.), *Proceedings of FRP Composite in Civil Engineering*, 12–15 December 2001, Hong Kong, China, Vol. 2, pp. 1247–1254.

Tan, K. H., Patoary, M. K. H., & Roger, C. S. K. (2003). Anchorage system for masonry walls strengthened with FRP composite laminates. *Journal of Reinforced Plastics and Composites*, *22*(15), 1353–1371.

Tan, K. H. (2002). Strength enhancement of rectangular reinforced concrete columns using fiber-reinforced polymer. *ASCE Journal Composite for Construction, 6*(3), 175–183.

Tan, K. H. (2003). Effect of cyclic loading on FRP-concrete interfacial bond strength. In *Proceedings of International Symposium on Latest Achievement of Technology and Research on Retrofitting Concrete structures*, JCI, Kyoto, July 2003, pp. 1–8.

Zhang, H., & Smith, S. (2012a). Influence of FRP anchor fan configuration and dowel angle on anchoring FRP plates. *Composites Part B Engineering, 43*(8), 3516–3527.

Zhang, H., & Smith, S. (2012b). FRP-to-concrete joint assemblages anchored with multiple FRP anchors. *Composite Structures*, *94*(2), 403–414.

Zehetmaier, Z. (2000). Entwicklung mechanischer endverankerungen für aufgeklebte CFK-lamellen. (Development of mechanical anchorages for externally bonded CFRP-strips). In K. Zilch (Ed.), Massivbau 2000, Forschung, Entwicklungen und Anwendungen, Münchner Massivbau- Seminar 2000, pp. 217–232. Springer VDI Verlag, Düsseldorf.

Mechanically Fastened Systems

Arora, D. (2003). Rapid Strengthening of Reinforced Concrete Bridge with Mechanically Fastened Fiber-Reinforced Polymer Strips. M.Sc. Thesis, University of Wisconsin, Madison, 353 pp.

Bank, L. C., Lamanna, A. J., Ray, J. C. & Velazquez, G. I. (2002). Rapid Strengthening of Reinforced Concrete Beams with Mechanically Fastened, Fiber Reinforced Polymeric Composites Materials. Report ERDC/GSL TR-02-4, US Army Corps of Engineers, 99 pp.

Bank, L. C. (2004). Mechanically-Fastened FRP (MF-FRP): A Viable Alternative for Strengthening RC Members. *Proceedings of the FRP Composites in Civil Engineering (CICE 2004), Adelaide, Australia*. December 8–10.

Bank, L. C., Arora, D. (2007). Analysis of RC beam strengthened with mechanically fastened FRP (MF-FRP) strips. *Composite Structures, 79*, 180–191.

Brown, V. L., Bank, L. C., Arora, D., Borowicz, D. T., Godat, A., Lamanna, A. J., Lee, J., Matta, F., Napoli, A. & Tan, K. H. Experimental Studies of Mechanically-Fastened FRP Systems: State-of-the-Art. ACI Special Publication-Proceedings of the FRPRCS-10. Tampa Bay, FL, USA, April 2011.

Dempsey, D. D., & Scott, D. W. (2006). Wood members strengthened with mechanically fastened FRP strips. *Journal of Composites for Construction, 10*(5), 392–398.

Ebead, U. (2011). Hybrid externally bonded/mechanically fastened fiber-reinforced polymer for RC beam strengthening. *ACI Structural Journal, 108*(6), 669–678.

Ekenel, M., Rizzo, A., Myers, J. J. & Nanni, A. (2005). Effect of fatigue loading on flexural performance of reinforced concrete beams strengthened with FRP fabric and pre-cured laminate systems. *Proceedings of 3rd International Conference of Composites in Construction*, Lyon, France.

Ekenel, M., Rizzo, A., Myers, J. J., & Nanni, A. (2006). Flexural fatigue behavior of reinforced concrete beams strengthened with FRP fabric and precured laminate systems. *Journal of Composites for Construction, 10*(5), 433–442.

Elsayed, W. E., Ebead, U. A., & Neale, K. W. (2009a). Studies of mechanically fastened fiber-reinforced polymer strengthening systems. *ACI Structural Journal, 106*, 49–59.

Elsayed, W. E., Ebead, U. A., & Neale, K. W. (2009b). Mechanically fastened FRP-strengthened two-way concrete slabs with and without cutouts. *Journal of Composites for Construction, 13* (1), 198–207.

El-Maaddawy, T. (2013). Mechanically fastened composites for retrofitting corrosion-damaged reinforced-concrete beams: experimental investigation. *Journal of Composites for Construction*, 1–9. ISSN 1090-0268/04013041(9).

Faella, C., Martinelli, E., & Nigro, E. (2008). Analysis of steel-concrete composite PR-frames in partial shear interaction: a numerical model and some applications. *Engineering Structures, 30* (4), 1178–1186.

Galati, D., Rizzo, A. & Micelli, F. (2007). Comparison of reinforced concrete beams strengthened with FRP pre-cured laminate systems and tested under flexural loading. *Proceedings of the 8th International Symposium on Fiber-Reinforced Polymer Reinforcement for Concrete Structures, FRPRCS-8*, Patras, Greece.

Johnson, D. (2011). An Investigation for Strengthening Existing Reinforced Concrete Beams in Shear Using a MF-FRP Retrofit System. Master Thesis 2011, University of Wisconsin-Madison, USA. pp. 1–202.

Lamanna, A. J., Bank, L. C., & Scott, D. W. (2001). Flexural strengthening of reinforced concrete beams using fasteners and fiber reinforced polymer strips. *ACI Structural Journal, 98*(3), 368–376.

Lamanna, A. J. (2002). Flexural Strengthening of Reinforced Concrete Beams with Mechanically Fastened Fiber Reinforced Polymer Strips. Ph.D. Dissertation, University of Wisconsin-Madison.

Lamanna, A. J., Bank, L. C., & Scott, D. W. (2004a). Flexural strengthening of reinforced concrete beams by mechanically attaching fiber-reinforced polymer strips. *Journal of Composites for Construction, 8*(3), 203–210.

Lamanna, A. J., Bank, L. C., & Borowicz, D. T. (2004b). Mechanically fastened FRP strengthening of large scale RC bridge T beams. *Advances in Structural Engineering, 7*(6), 525–538.

Lee, H. L., Lopez, M. M., Bakis, C. E. Flexural behavior of reinforced concrete beams strengthened with mechanically fastened FRP strip. *Proceedings of FRPRCS-8. Patras, Greece*, pp. 1–9.

Lee, J. H., Lopez, M. M., & Bakis, C. E. (2009). Slip effects in reinforced concrete members with mechanically fastened FRP strip. *Cement and Concrete Composites, 31*, 496–504.

Martin, J. A., & Lamanna, A. J. (2008). Performance of mechanically fastened FRP strengthened concrete beams in flexure. *Journal of Composites for Construction, 12*(3), 257–265.

Martinelli, E., Napoli, A., Nunziata, B. & Realfonzo, R. (2013). Flexural Response of RC Beams Strengthened by MF-FRP Laminates: Numerical Modeling. *Proceedings of SMAR 2013, Istanbul*, September 9–11.

Martinelli, E., Napoli, A., Nunziata, B., & Realfonzo, R. (2014). A 1D finite element model for the flexural behaviour of RC beams strengthened with MF-FRP strips. *Composite Structures, 107*, 190–204.

Napoli, A., Matta, F., Martinelli, E., Nanni, A., & Realfonzo, R. (2010). Modeling and verification of response of RC slabs strengthened in flexure with mechanically fastened FRP laminates. *Magazine of Concrete Research, 62*(8), 593–605.

Napoli, A., Bank, L. C., Brown, V. L., Martinelli, E., Matta, F., & Realfonzo, R. (2013). Analysis and design of RC structures strengthened with mechanically fastened FRP laminates: a review. *Composites Part B: Eng, 55*, 386–399.

Nardone, F., Lignola, G. P., Prota, A., Manfredi, G. & Nanni, A. (2012) Ultimate limit state of MF-FRP beams. In Biondini & Frangopol (Eds.), *Proceedings "6th International Conference on Bridge Maintenance, Safety and Management (IABMAS 2012). Stresa, Lake Maggiore*, Italy, July 8–12, pp. 1235–1242. London: Taylor & Francis Group. ISBN 978-0-415-62124-3.

Nardone, F., Lignola, G. P., Prota, A., Manfredi, G., & Nanni, A. (2011). Modeling of flexural behavior of RC beams strengthened with mechanically fastened FRP strips. *Elsevier Composite Structures, 93*(8), 1973–1985.

Newmark, N. M., Siess, C. P. & Viest, I. M. (1951). Tests and Analysis of Composite Beams with Incomplete Interaction. *Proceedings of the Society of Experimental Stress Analysis* (Vol. 9, no. 1, pp. 75–92).

Oliva, M., Bank. L. C., Borowicz, D. T., Arora, D. (2003). Rapid strengthening of reinforced concrete bridges. Technical Report 2003, University of Wisconsin Madison, Wisconsin Highway Research Program, USA. pp. 1–167.

Quattlebaum, J. B., Harries, K. A., & Petrou, M. F. (2005). Comparison of three flexural retrofit systems under monotonic and fatigue loads. *Journal of Bridge Engineering, 10*(6), 731–740.

Realfonzo, R., Martinelli, E., Napoli, A., & Nunziata, B. (2013). Experimental investigation of the mechanical connection between FRP laminates and concrete. *Composites Part B Engineering, 45*(1), 341–355.

Rizzo, A. (2005). Application of Mechanically Fastened FRP (MF-FRP) Pre-cured Laminates in Off- System Bridges. MSc thesis, University of Missouri-Rolla, USA. pp. 1–285.

Rizzo, A., Galati, N., Nanni, A. & Dharani, L. R. (2005a). Material Characterization of FRP Pre-Cured Laminates Used in the Mechanically Fastened FRP Strengthening of RC Structures. SP-230. *7th International Symposium on Fiber-Reinforced (FRP) Polymer Reinforcement for Concrete Structures, American Concrete Institute* (Vol. 230, pp. 135-152).

Rizzo, A., Galati, N., Nanni, A. & Bank, L. C. (2005b). Strengthening Concrete Structures with Mechanically Fastened Pultruded Strips. *Proceedings of Composites*. Columbus, Ohio, USA, September 28–30.

Rosner, C. N., & Rizkalla, S. H. (1995). Bolted connections for fiber reinforced composite structural members: experimental program. *Journal of Materials in Civil Engineering, 7*(4), 223–231.

Schorer, A. E., Bank, L. C., Oliva, M. G., Wacker, J. P. & Rammer, D. C. (2008). Feasibility of Rehabilitating Timber Bridges Using Mechanically Fastened FRP Strips. *Proceedings of the ASCE SEI Structures 2008 Conference: Crossing Borders, Vancouver, Canada*, April 24–26, 2008.

Sena-Cruz, J. M., Barros, J. A. O., Coelho, M. R. F. & Silva, L. F. F. T. (2011). Efficiency of different techniques in flexural strengthening of RC beams under monotonic and fatigue loading. *Construction and Building Materials*, *29*, 175–182.